Received: 7 April 2020 | Revised: 14 October 2020 | Accepted: 15 October 2020

DOI: 10.1002/eqe.3382

WILEY

RESEARCH ARTICLE

Earthquake input and state estimation for buildings using absolute floor accelerations

Sdiq Anwar Taher[1] | **Jian Li**[1] | **Huazhen Fang**[2]

[1] Department of Civil, Environmental and Architectural Engineering, The University of Kansas, Lawrence, Kansas

[2] Department of Mechanical Engineering, The University of Kansas, Lawrence, Kansas

Correspondence
Jian Li, Ph.D., P.E., Associate Professor, Department of Civil, Environmental and Architectural Engineering, The University of Kansas, Lawrence, KS 66045.
Email: jianli@ku.edu

Abstract

After earthquakes, structural response such as interstory drift is critical for accurate structural assessment for buildings. Typically, direct integration of absolute floor accelerations does not yield reliable floor displacements due to the long-period drifts caused by noise, a widely acknowledged challenge. In this case, model-based estimation strategies can be employed, which often require the ground input for better accuracy. However, in many cases the ground input may not be available for lack of instrumentation or even be unmeasurable due to soil-structure interaction, hence needs to be estimated. Earthquake input estimation in this case is particularly challenging due to the lack of direct feedthrough term, leading to low observability of system input. As a result, input estimation is sensitive to modeling error, measurement noise, and incomplete measurements. To address this challenge, a hybrid strategy is proposed to estimate earthquake input, states, and acceleration response at unmeasured floors using limited absolute floor acceleration measurements. First, the earthquake input is estimated through a maximum a posteriori (MAP) estimation method, and then the estimated input is combined with Kalman filter to further estimate states and unmeasured responses. A comprehensive assessment was performed through a series of numerical and experimental tests including a comparative study with a popular online model-based method. While the online method demonstrated certain sensitivity to modeling error and measurement noise due to weak observability, the proposed strategy showed robustness and accuracy under realistic and challenging conditions. Further verification is also performed using a real-world building structure that experienced earthquake events.

KEYWORDS

absolute acceleration, Bayesian inference, earthquake excitation, incomplete measurement, input estimation, Kalman filter, maximum a *posteriori*, measurement noise, modeling error, shear building, state estimation

1. | INTRODUCTION

In seismic zones, strong ground motions caused by earthquakes pose one of the greatest threats to civil structures such as buildings.[1,2] After major earthquakes, effective structural assessment is critical to understanding structural integrity in order to support informed postdisaster decision-making.[3] For multistory building structures, interstory drift has been

recognized as an effective performance index,[4] and has been widely used for story damage assessment.[5] However, direct measurement of interstory drift during earthquakes is challenging since floor displacements are not easily measurable in real-world buildings.[6] Although sensors for direct measurement of interstory drift have been developed and studied based on laser[7,8] and photonic sensor,[5] they are not yet widely available in practice. Therefore, indirect floor displacement estimation has been explored using structural responses that can be directly measured such as accelerations. Another challenge is that sensor instrumentation is often limited, which is the case for most buildings instrumented by the California Strong Motion Instrumentation Program (CSMIP), leading to incomplete picture of building response formed by a small number of floors. In this case, the Kalman Filter,[9] a model-based estimation method, can be used to estimate unmeasured states (eg, displacements) and acceleration responses using limited acceleration measurements.

However, the above Kalman Filter-based approach requires the input information, that is, the earthquake excitation, to be measured. For building structures, although the input ground motion can often be directly measured using seismographs or accelerometers, due to the cost of instrumentation, some buildings equipped with structural health monitoring systems may only focus on structural response monitoring,[10] hence the ground input would not be measured should earthquakes occur. Free-field ground motions measured at a nearby site is often quite different from the real input to the building due to attenuation and filtering through the soil.[11] Even if instrumentation is available at the ground floor, sensor failure may occur, leading to unknown input information. Moreover, in some cases, the real ground input to the structure is virtually impossible to measure directly due to kinematic interaction effects of soil-structures interaction.[12] As a result, estimating floor displacements and hence interstory drifts remains a challenge.

In terms of earthquake input estimation, earlier efforts were focused on reconstructing unknown earthquake inputs and estimating unknown structural parameters at the same time. For example, Li and Chen[13] proposed a statistical average algorithm to estimate structural parameters and ground motion excitation of a discrete multidegree-of-freedom linear system formulated in relative coordinates, that is, motion with respect to the ground. As a result, the response measurements needed for applying the algorithm, including acceleration, velocity, and displacement, must be obtained in relative coordinates. Zhao et al.[14,15] developed a hybrid identification method under absolute coordinates to identify structural parameters and ground input of multistory buildings. It also assumed that all structural responses including acceleration, velocity, and displacement are available. Since accelerations are measured in absolute coordinates and full structural responses are rarely available in practice, the applicability of the aforementioned methods for ground input estimation is limited.

In recent years, combined deterministic-stochastic methods for online joint input-state estimation have been explored, which consider uncertainties in the state variables and measurements. A number of Kalman filter-based algorithms were presented to identify both states and inputs together for linear systems with direct feedthrough, such as structures directly loaded with forces. Lourens et al.[16] proposed an augmented Kalman filter (AKF) algorithm for force identification in which unknown forces are incorporated in the state vector in order to identify them together. The algorithm was experimentally investigated using a cantilever beam with an unknown tip load. When only acceleration measurements were used, the algorithm was found unstable[17] due to unobservability of input in the augmented system formulation.[16,24] To tackle the problem, dummy-measurement[17] and heterogeneous structural measurements such as strain and acceleration[18] were included in the input and state estimation with AKF. Gillijns and De Moor[19] developed a Kalman filter-based joint input and state estimation algorithm for linear discrete-time systems with direct feedthrough. The algorithm was later applied in structural dynamics using reduced-order models with a limited number of acceleration measurements for force identification, and was examined through a numerical example, a laboratory experiment, and in-situ experiment on a footbridge.[20] The extension of the algorithm with proven stability properties was proposed in Ref. (21). Subsequently, Maes et al.[22,23] presented further improvement by incorporating displacement in addition to acceleration measurements as well as the effect of unknown stochastic force, for example, wind loads. Azam et al.[24] developed a dual Kalman filter approach (DKF) for linear systems with direct feedthrough. The approach was applied to identify state and force input from acceleration measurements in numerical simulations.

However, for earthquake-excited building structures, the fact that floor responses are measured in terms of absolute accelerations renders the system without direct feedthrough, leading to weak observability of the system input. Several Kalman filter-based methods have been proposed for joint input-state estimation of systems without direct feedthrough. For example, a Kalman filter-based joint input and state estimation algorithm for linear discrete-time systems, hereinafter referred to as the Gillijns Algorithm, was proposed by Gillijns and De Moor.[25] The algorithm was designed to estimate input and state for systems without direct feedthrough. However, as will be shown later in this paper, for earthquake-excited building structures with absolute floor acceleration measurements, this method is sensitive to measurement noise, modeling error, and incomplete measurements. Tuan et al.[26] proposed to use Kalman filter and a separate recursive

least-squares algorithm to estimate input of an inverse heat conduction problem. The algorithm was then applied by Liu et al.[27] and Ma et al.[28] to identify the input force of a cantilever plate and beam through numerical simulations and experimental testing. Wu et al.[29] later applied Tuan's algorithm to estimate the soil-pile interaction forces during shake table tests, which, however, requires full response measurements. More recently, Nayek et al.[30] introduced a Gaussian process latent force model into AKF for joint input-state estimation in case of wind and earthquake loadings using absolute floor acceleration measurements. However, the structural model was assumed to be accurate so the robustness against modeling error is unclear. In summary, although there have been some Kalman filter-based approaches for joint input-state estimation of systems without direct feedthrough, the weak observability of system input makes the estimation sensitive to measurement noise, modeling error, and incomplete measurements. As a result, a robust strategy is still lacking to estimate unknown earthquake input and unmeasured floor responses using limited absolute floor acceleration measurements.

On the other hand, offline strategies have been widely applied to tackle the ill-posed inverse problem of input estimation, such as the least squares-based methods with Tikhonov regularization or maximum a *posteriori* (MAP) estimation method[31–33] and Bayesian inference.[34–37] For example, Tikhonov regularization was applied to estimate unknown inputs through various forms including (1) an average acceleration discrete algorithm,[31] (2) an explicit form of the Newmark-β method,[32] and (3) a state space formulation.[33] Feng et al.[34] presented the identification of structural parameters and moving vehicle loads using the MAP method and Bayesian inference proposed in Refs. (36–38). The approach presented in Ref. (34) was verified through numerical examples with a single-span simply supported bridge and a three-span continuous bridge. Note that the advantage of the MAP method and Bayesian inference, compared with other approaches, for example, the L-curve method,[39] is the ability to effectively find optimal regularization parameters for large matrices to address the ill-posed inverse problem.[34–38] Generally, these methods have produced satisfactory results of external input estimations for both moving and nonmoving forces.

This paper aims at performing reliable input and state estimation for earthquake-excited building structures using absolute accelerations measured at a limited number of floors. First, the problem formulation is presented in linear state-space form. The fact that absolute floor accelerations are measured renders the system without direct feedthrough, which in turn leads to weak observability of the system input. The challenges of identifying input for earthquake-excited building structures are then discussed. The rest of the paper is summarized in terms of the main contributions of this study, which include: (1) proposing a hybrid strategy that combines maximum a *posteriori* (MAP) estimation method coupled with Bayesian inference and Kalman filter to perform input and state estimation. Specifically, the MAP method, which can improve the condition of the inverse problem hence the robustness of the solution against modeling error and measurement noise, is applied to estimate the ground input, which is further combined with the floor acceleration measurements to estimate unmeasured floor responses such as accelerations, velocities, and displacements using Kalman filter. (2) Performing a comprehensive assessment of the proposed method numerically by considering different levels of modeling error, measurement noise, and incomplete instrumentation. A comparison is also performed between the proposed method and the online method by Gillijns and De Moor.[25] (3) Validating the proposed method using experimental and field data through testing a six-story lab-scale building structure and strong motion data measured from one of the buildings instrumented by CSMIP.

2. | PROBLEM FORMULATION

2.1. | Equation of motion in relative coordinates

For earthquake-excited building structures, the equation of motion is commonly formulated in relative coordinates as:

$$\mathbf{M}\ddot{\mathbf{u}}_r(t) + \mathbf{C}\dot{\mathbf{u}}_r(t) + \mathbf{K}\mathbf{u}_r(t) = -\mathbf{M}\mathbf{L}\ddot{\mathbf{u}}_g(t), \tag{1}$$

where $\mathbf{M}$, $\mathbf{C}$, and $\mathbf{K} \in \mathbb{R}^{n\times n}$ are the mass, damping, and stiffness matrices, respectively. Further, n is the number of degrees of freedom (DOF), $\ddot{\mathbf{u}}_g(t) \in \mathbb{R}$ is the ground acceleration input vector, $\mathbf{L} \in \mathbb{R}^n$ is the ground input selection vector, in which $\mathbf{L}$ equals to $[1, 1, \ldots, 1]^T$, and $\ddot{\mathbf{u}}_r$, $\dot{\mathbf{u}}_r$, and $\mathbf{u}_r \in \mathbb{R}^n$ are the relative acceleration, velocity, and displacement vectors for the floors, respectively, with respect to the ground. Note that in this study, the structure is assumed to remain linear during the earthquake excitation, allowing the adoption of a linear governing equation.

2.2. | State space formulation

2.2.1. | Continuous-time state space model

Equation (1) can be re-written in a continuous-time state space form:

$$\dot{\mathbf{x}}(t) = \mathbf{A}_c \mathbf{x}(t) + \mathbf{B}_c \ddot{\mathbf{u}}_g(t) \tag{2}$$

with

$$\mathbf{A}_c = \begin{bmatrix} 0 & \mathbf{I} \\ -\mathbf{M}^{-1}\mathbf{K} & -\mathbf{M}^{-1}\mathbf{C} \end{bmatrix}, \quad \text{and} \quad \mathbf{B}_c = \begin{bmatrix} 0 \\ -\mathbf{L} \end{bmatrix}. \tag{3}$$

In above, $\mathbf{x}(t) \in \mathbb{R}^{n_s}$ is the state vector, $\mathbf{A}_c \in \mathbb{R}^{n_s \times n_s}$ and $\mathbf{B}_c \in \mathbb{R}^{n_s \times n_d}$ are the system matrix and input vector, respectively, and $\mathbf{I} \in \mathbb{R}^{n \times n}$ is the identity matrix, n_s and n_d are the number of states and inputs, respectively. Here, n_d is equal to 1 for one-directional earthquake input. The state vector $\mathbf{x}(t)$ contains the relative displacement and velocity vectors:

$$\mathbf{x}(t) = \begin{bmatrix} \mathbf{u}_r(t) \\ \dot{\mathbf{u}}_r(t) \end{bmatrix}. \tag{4}$$

In general, the measurement vector $\mathbf{y}_t(t)$ can be written as a linear combination of the acceleration, velocity, and displacement vectors:

$$\mathbf{y}_t(t) = \boldsymbol{S}_a \ddot{\mathbf{u}}_r(t) + \boldsymbol{S}_v \dot{\mathbf{u}}_r(t) + \boldsymbol{S}_d \mathbf{u}_r(t) \tag{5}$$

in which $\boldsymbol{S}_a, \boldsymbol{S}_v$, and $\boldsymbol{S}_d \in \mathbb{R}^{n_d \times n}$ are the output influence matrices for acceleration, velocity, and displacement, respectively, with n_d the number of measurements. Assuming that the relative acceleration responses are measured, the measurement equation can be rewritten as$\mathbf{y}_r(t) = \boldsymbol{S}_a \ddot{\mathbf{u}}_r$. Thus, combining Equation (1), the measurement equation can be formulated as:

$$\mathbf{y}_r(t) = \mathbf{C}_c \mathbf{x}(t) + \mathbf{D}_c \ddot{\mathbf{u}}_g(t) \tag{6}$$

with

$$\mathbf{C}_c = \left[-\boldsymbol{S}_a \mathbf{M}^{-1}\mathbf{K} \quad -\boldsymbol{S}_a \mathbf{M}^{-1}\mathbf{C} \right], \quad \text{and} \quad \mathbf{D}_c = \left[-\boldsymbol{S}_a \mathbf{L} \right], \tag{7}$$

where $\mathbf{C}_c \in \mathbb{R}^{n_d \times n_s}$ and $\mathbf{D}_c \in \mathbb{R}^{n_d \times 1}$ are the output matrix and direct feedthrough vector, respectively. However, in practical applications, absolute acceleration responses are measured, rather than relative accelerations. Therefore, the ground acceleration should be added to the measurement Equation (6). As a result, the direct feedthrough vector vanishes, leading to absolute acceleration measurements of the building floors expressed as

$$\mathbf{y}(t) = \mathbf{C}_c \mathbf{x}(t), \tag{8}$$

where $\mathbf{y}(t)$ is the absolute acceleration measurements. Note that Equation (8) is the measurement equation used in the subsequent discussions. However, Equations (5)-(7) are included here to highlight the fact that accelerations are measured in absolute coordinates, leading to no direct feedthrough.

2.2.2. | Discrete-time state space model

Equations (2) and (8) can be converted to discrete-time domain through the zero-order hold method as

$$\mathbf{x}_{[k+1]} = \mathbf{A}_d \mathbf{x}_{[k]} + \mathbf{B}_d \ddot{\mathbf{u}}_{g[k]} + \mathbf{w}_{[k]}, \tag{9}$$

$$\mathbf{y}_{[k]} = \mathbf{C}_d \mathbf{x}_{[k]} + \mathbf{v}_{[k]}, \tag{10}$$

in which $\mathbf{x}_{[k]} = \mathbf{x}(k\Delta t)$, $\mathbf{y}_{[k]} = \mathbf{y}(k\Delta t)$, and $\ddot{\mathbf{u}}_{\mathbf{g}[k]} = \ddot{\mathbf{u}}_{\mathbf{g}}(k\Delta t)$, with $k = 1, 2, \ldots, n_t$, Δt is the sample time, and n_t is the total number of data points. $\mathbf{w}_{[k]}$ and $\mathbf{v}_{[k]}$ are added to consider the process noise and measurement noise, respectively. The vectors $\mathbf{w}_{[k]}$ and $\mathbf{v}_{[k]}$ are assumed to be zero-mean Gaussian white noise with known covariance matrices $\mathbb{E}[\mathbf{v}_{[k]}\mathbf{v}_{[l]}^T] = \mathbf{R}\delta(k,l)$ with $\mathbf{R} > 0$ and $\mathbb{E}[\mathbf{w}_{[k]}\mathbf{w}_{[l]}^T] = \mathbf{Q}\delta(k,l)$ with $\mathbf{Q} \geq 0$, which are mutually uncorrelated ($\mathbb{E}[\mathbf{v}_{[k]}\mathbf{w}_{[l]}^T] = 0$). The discrete-time system matrices $\mathbf{A}_d$, $\mathbf{B}_d$, and $\mathbf{C}_d$ are given by

$$\mathbf{A}_d = \mathbf{exp}\left(\mathbf{A}_c\Delta t\right), \mathbf{B}_d = \mathbf{A}_c^{-1}\left(\mathbf{A}_d - \mathbf{I}_{n_s}\right)\mathbf{B}_c, \mathbf{C}_d = \mathbf{C}_c \tag{11}$$

in which $\mathbf{I}_{n_s} \in \mathbb{R}^{n_s \times n_s}$ is the identity matrix.

2.3. | Challenge of input estimation for ground-excited building structures

Model-based input estimation using output measurements is intrinsically an inverse problem. Therefore, the accuracy and numerical condition of the system model play a critical role in the accuracy and robustness of the estimation. In particular, if the numerical condition of the system model is weak (high condition number), the uncertainties of the measurement and model may leave a big impact on the estimation, for which a small change in the measurement and model would result in a drastic change in the estimation. In fact, there are always uncertainties in measurements in practice, which further lead to inaccuracies of model $[\mathbf{A}_d, \mathbf{B}_d, \mathbf{C}_d]$ constructed using these measurements. Despite the consideration of measurement and model uncertainties in the existing methods for state and input estimation, depending on applications, applicability of these methods is still limited to a certain level of measurement noise and modeling error. Here, the challenge of input estimation for ground-excited building structures is discussed based on the numerical condition of the observability matrix.

Substituting Equation (9) into Equation (10), the measurement equation $\mathbf{y}_{[k]}$ can be rewritten in a matrix form as

$$\boldsymbol{Y} = \boldsymbol{O}\mathbf{x}_{[0]} + \boldsymbol{H}\ddot{\boldsymbol{U}}_g = [\boldsymbol{OH}]\begin{bmatrix}\mathbf{x}_{[0]} \\ \ddot{\boldsymbol{U}}_g\end{bmatrix} \tag{12}$$

in which

$$\boldsymbol{O} = \begin{bmatrix}\mathbf{C}_d \\ \mathbf{C}_d\mathbf{A}_d \\ \vdots \\ \mathbf{C}_d\mathbf{A}^L{}_d\end{bmatrix}, \boldsymbol{H} = \begin{bmatrix}0 & 0 & \cdots & 0 \\ \mathbf{C_d}\mathbf{B_d} & 0 & \cdots & 0 \\ \vdots & \vdots & \ddots & \vdots \\ \mathbf{C_d}\mathbf{A_d}^{\mathbf{L-1}}\mathbf{B_d} & \mathbf{C_d}\mathbf{A_d}^{\mathbf{L-2}}\mathbf{B_d} & \cdots & \mathbf{C_d}\mathbf{B_d}\end{bmatrix}, \tag{13}$$

$$\boldsymbol{Y} = \begin{bmatrix}\mathbf{y}_{[0]}^T & \mathbf{y}_{[1]}^T & \cdots & \mathbf{y}_{[L]}^T\end{bmatrix}^T, \ldots \ddot{\boldsymbol{U}}_g = \begin{bmatrix}\ddot{\mathbf{u}}_{\boldsymbol{g}[0]}^T & \ddot{\mathbf{u}}_{\boldsymbol{g}[1]}^T & \cdots & \ddot{\mathbf{u}}_{\boldsymbol{g}[L-1]}^T\end{bmatrix}^T, \tag{14}$$

where $\boldsymbol{\Gamma} = [\boldsymbol{O}\ \boldsymbol{H}] \in \mathbb{R}^{n_d(L+1)\times(n_s+L)}$ is the observability matrix of the system input and L is the number of sampled data points. To ensure the system is observable, the matrix $\boldsymbol{\Gamma}$ must be full column rank. In addition, the numerical condition of the observability matrix $\boldsymbol{\Gamma}$ affects the degree of observability.[40] From the literature, the following two definitions can be expressed:

Definition 1: The system $(\mathbf{A}_d, \mathbf{C}_d)$ is observable if $\boldsymbol{O}$ has full column rank such that $\mathbf{x}_{[0]}$ can be uniquely determined.

Definition 2: The system $(\mathbf{A}_d, \mathbf{B}_d, \mathbf{C}_d)$ is observable if $\boldsymbol{\Gamma}$ has full column rank such that $\mathbf{x}_{[0]}$ and $\ddot{\boldsymbol{U}}_g$, $[\begin{smallmatrix}\mathbf{x}_{[0]} \\ \ddot{\boldsymbol{U}}_g\end{smallmatrix}]$, can be uniquely determined.

State observability as in *Definition 1* would provide a guarantee for the Kalman filter to succeed in state estimation. Similarly, if the observability condition in *Definition 2* is satisfied, effective input and state estimation will be achieved. For earthquake-excited building structure considered in this study, based on our observation, if $\boldsymbol{Y}$ contains absolute floor acceleration measurements, $\boldsymbol{\Gamma}$ is often of full column rank. However, the numerical condition of $\boldsymbol{\Gamma}$ is weak. In other words, $\boldsymbol{\Gamma}$ has a very large ratio between its largest and smallest singular values, leading to low degree of observability, or weak observability. Due to weak observability, existing approaches for input and state estimation using earthquake-excited building structure systems may be sensitive to measurement noise, modelling error, and incomplete measurement,[41] as

will be demonstrated in Section 3.4. Therefore, it is still challenging to identify both input and states using absolute floor acceleration measurements for earthquake-exciting building structures.

2.4. | A hybrid strategy for input and state estimation

In the presence of noise, modeling error, and incomplete absolute acceleration measurements, input and state estimation for earthquake-excited building structures is still challenging due to weak observability. In this paper, a two-step strategy is proposed which consists of a maximum a *posterior* (MAP) estimation approach and Kalman filtering to estimate input and state for building structures utilizing a limited number of absolute acceleration measurements.

2.4.1. | Input reconstruction

The proposed strategy is based on maximum *a posteriori* (MAP) estimation approach to estimate the ground input in the first step using an offline strategy. After applying zero initial conditions and removing the first row of $\boldsymbol{H}$ matrix considering $L = n_t$, Equation (12) can be rewritten as:

$$\boldsymbol{Y} = \boldsymbol{H}\ddot{\boldsymbol{U}}_g, \tag{15}$$

where $\boldsymbol{Y} \in \mathbb{R}^{n_d n_t \times 1}$ is the collected absolute acceleration response vector,$\ddot{\boldsymbol{U}}_g \in \mathbb{R}^{n_t \times 1}$ is the ground input vector, and $\mathbf{H} \in \mathbb{R}^{n_d\ n_t \times n_t}$ is the lower-block triangular Hankel matrix[42] which contains the system Markov parameters.

From Equation (15), the unknown ground input vector $\ddot{\boldsymbol{U}}_g$ can be solved using maximum *a posteriori* estimation (MAP) which includes prior information of input to improve the condition number of the $\boldsymbol{H}$ matrix. The MAP approach for Equation (15) considers the following problem:

$$\ddot{\boldsymbol{U}}_g = \mathbf{arg\,max}\ p(\ddot{\boldsymbol{U}}_g|\boldsymbol{Y}) \tag{16}$$

From Bayes' rule,

$$p\left(\ddot{\boldsymbol{U}}_g|\boldsymbol{Y}\right) = \frac{p\left(\boldsymbol{Y}|\ddot{\boldsymbol{U}}_g\right) p\left(\ddot{\boldsymbol{U}}_g\right)}{p\left(\boldsymbol{Y}\right)} \propto p\left(\boldsymbol{Y}|\ddot{\boldsymbol{U}}_g\right) p\left(\ddot{\boldsymbol{U}}_g\right), \tag{17}$$

where $p(\ddot{\boldsymbol{U}}_g|\boldsymbol{Y})$ is the posteriori probability density function, $p(\boldsymbol{Y}|\ddot{\boldsymbol{U}}_g)$ is the likelihood function, and $p(\ddot{\boldsymbol{U}}_g)$ is the prior probability density function which helps to improve the condition of the $\boldsymbol{H}$ matrix. If $\boldsymbol{Y} = \boldsymbol{H}\ddot{\boldsymbol{U}}_g + \boldsymbol{e}$, in which $\boldsymbol{e}$ is the prediction error with $\boldsymbol{e} \sim \mathcal{N}(0, \sigma^2\boldsymbol{I})$. $p(\boldsymbol{Y}|\ddot{\boldsymbol{U}}_g)p(\ddot{\boldsymbol{U}}_g)$ can be formulated as

$$p\left(\boldsymbol{Y}|\ddot{\boldsymbol{U}}_g\right) p\left(\ddot{\boldsymbol{U}}_g\right) \propto \exp\left(-\frac{1}{2\sigma^2}\left[\boldsymbol{Y} - \boldsymbol{H}\ddot{\boldsymbol{U}}_g\right]^T\left[\boldsymbol{Y} - \boldsymbol{H}\ddot{\boldsymbol{U}}_g\right]\right) \exp\left(-\frac{\tau}{2}\ddot{\boldsymbol{U}}_{\boldsymbol{g}}^T\ddot{\boldsymbol{U}}_g\right). \tag{18}$$

In which τ is a scale parameter of the input. Based on the log of Equation (18), the following cost function can be written:[36,37]

$$J\left(\ddot{\boldsymbol{U}}_g\right) = \frac{1}{2\sigma^2}\left[\boldsymbol{Y} - \boldsymbol{H}\ddot{\boldsymbol{U}}_g\right]^T\left[\boldsymbol{Y} - \boldsymbol{H}\ddot{\boldsymbol{U}}_g\right] + \frac{\tau}{2}\ddot{\boldsymbol{U}}_{\boldsymbol{g}}^T\ddot{\boldsymbol{U}}_g. \tag{19}$$

The solution to minimizing Equation (19) is given by

$$\widehat{\ddot{\boldsymbol{U}}}_g = \left(\lambda\mathbf{I} + \boldsymbol{H}^T\boldsymbol{H}\right)^{-1}\boldsymbol{H}^T\boldsymbol{Y}, \tag{20}$$

where $\lambda = \tau\sigma^2$, in which τ and σ^2 are considered as random variables and inferred through a Bayesian framework as will explained in *Remark 1*. Similar to $\boldsymbol{\Gamma}$ discussed in Section 2.3, $\boldsymbol{H}$ is full column rank, but is poorly conditioned, leading to weak observability, in which a small change in $\mathbf{Y}$ would cause a significant change in $\widehat{\ddot{\boldsymbol{U}}}_g$. Here, λ of the MAP approach

helps to improve the condition number, leading to a more robust estimation. It is also noted that the MAP estimation provides a probabilistic interpretation of and is equivalent to the weighted least squares problem with Tikhonov regularization. Therefore, Equation (20) can be applied to estimate both Gaussian and non-Gaussian random inputs. Note that Equation (20) involves the inversion of a matrix whose dimension is related to the number of DOFs and the sampled data points. The computational cost could be high in case large DOF number and high sampling rate. In this case, gradient-based optimization could be employed to obtain the solution that minimizes Equation (19). For the numerical example shown in Section 3.2, the computational cost for input estimation is 1.37 seconds utilizing MATLAB program[43] through a PC with a 16 GB RAM and a Core i7-3520M CPU @ 2.9Hz.

Remark 1: The accuracy of $\widehat{\ddot{\boldsymbol{U}}}_g$ relies on the selection of λ. Hence, λ needs to be selected carefully. A small value, for example, between 0.01 and 1, for λ is recommended. In terms of optimality, there are several methods to select an optimal λ including the L-curve[39] and the so-called Bayesian inference[36–38] methods. In this paper, Bayesian inference was used to select the optimal λ. In particular, Equation (17) is augmented to include the prior distributions of τ and σ^2:

$$p\left(\ddot{\boldsymbol{U}}_g, \sigma^2, \tau | \boldsymbol{Y}\right) \propto p\left(\boldsymbol{Y} | \ddot{\boldsymbol{U}}_g, \sigma^2\right) p\left(\ddot{\boldsymbol{U}}_g | \tau\right)\ p\left(\sigma^2\right) p\left(\tau\right), \tag{21}$$

where $p(\sigma^2)$ and $p(\tau)$ are selected as conjugate priors that are expressed using Gamma distribution. Thus, a new cost function $J(\ddot{\boldsymbol{U}}_g, \sigma^2, \tau)$ is obtained. After solving the new cost function, τ and σ^2 are obtained as

$$\tau = \frac{\frac{1}{2}n_t + \alpha_0 - 1}{\frac{1}{2}\ddot{\boldsymbol{U}}_g^T \ddot{\boldsymbol{U}}_g + \beta_0} \quad \text{and} \quad \sigma^2 = \frac{\frac{1}{2}\left[\boldsymbol{Y} - \boldsymbol{H}\ddot{\boldsymbol{U}}_g\right]^T \left[\boldsymbol{Y} - \boldsymbol{H}\ddot{\boldsymbol{U}}_g\right] + \beta_1}{\frac{1}{2}n_d n_t + \alpha_1 + 1}, \tag{22}$$

where $\alpha_0, \beta_0, \alpha_1$, and β_1 are hyperparameters. From Equations (20) and (22), $\widehat{\ddot{\boldsymbol{U}}}_g$ is computed in an iterative manner, in which τ and σ^2 are automatically obtained. Details of the selection of the hyperparameters are discussed in Refs. (36)-(38).

2.4.2. | State estimation

With the reconstructed ground input, the state vector, which consists of the relative displacement and velocity, can be estimated using the classical Kalman filter.[9] After applying the initial state $\hat{\mathbf{x}}_{[0|-1]}$ and the initial error covariance $\mathbf{P}_{[0|-1]}$, the state vector $\hat{\mathbf{x}}_{[k|k]}$ is identified in two steps, including measurement update and time update using a limited number of absolute acceleration measurement vector $\mathbf{y}_{[k]}$ and the reconstructed ground input vector $\widehat{\ddot{\mathbf{u}}}_{g[k]}$ obtained from the MAP estimate. The statement estimation is given by the following equations:[44,45]

Measurement update:

$$\mathbf{K}_{[k]} = \mathbf{P}_{[k|k-1]}\mathbf{C}_{\boldsymbol{d}}^{\mathrm{T}}\left(\mathbf{C}_{\boldsymbol{d}}\mathbf{P}_{[k|k-1]}\mathbf{C}_{\boldsymbol{d}}^{\mathrm{T}} + \mathbf{R}\right)^{-1}, \tag{23}$$

$$\hat{\mathbf{x}}_{[k|k]} = \hat{\mathbf{x}}_{[k|k-1]} + \mathbf{K}_{[k]}(\mathbf{y}_{[k]} - \mathbf{C}_{\boldsymbol{d}}\hat{\mathbf{x}}_{[k|k-1]}), \tag{24}$$

$$\mathbf{P}_{[k|k]} = (\mathbf{I} - \mathbf{K}_{[k]}\mathbf{C}_{\boldsymbol{d}})\mathbf{P}_{[k|k-1]}, \tag{25}$$

$$\hat{\mathbf{y}}_{[k|k]} = \bar{\mathbf{C}}_{\boldsymbol{d}}\hat{\mathbf{x}}_{[k|k]}. \tag{26}$$

Time update:

$$\hat{\mathbf{x}}_{[k+1|k]} = \mathbf{A}_{\boldsymbol{d}}\hat{\mathbf{x}}_{[k|k]} + \mathbf{B}_{\boldsymbol{d}}\widehat{\ddot{\mathbf{u}}}_{g[k]}, \tag{27}$$

$$\mathbf{P}_{[k+1|k]} = \mathbf{A}_{\boldsymbol{d}}\mathbf{P}_{[k|k]}\mathbf{A}_{\boldsymbol{d}}^{\mathrm{T}} + \mathbf{Q}, \tag{28}$$

where $\mathbf{K}_{[k]}$ is Kalman gain, and $\hat{\mathbf{y}}_{[k]}$ and $\bar{\mathbf{C}}_{\boldsymbol{d}}$ are the estimated response vector and output matrix at unmeasured locations. A large value for the initial error covariance $\mathbf{P}_{[0|-1]}$ is recommended.

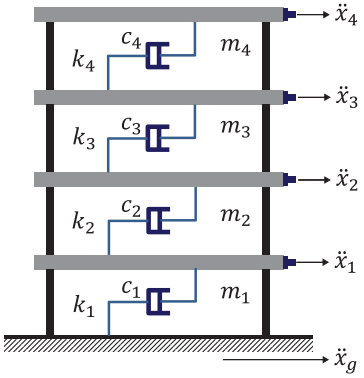

FIGURE 1 A four-story shear-type building model

Structural Parameters

Floor	Mass		Stiffness	
	kg×10^5	kip-sec^2/in	kN/m×10^5	kip/in
1	3.503	2.0	5.604	3200
2	3.503	2.0	4.203	2400
3	2.627	1.5	2.802	1600
4	2.627	1.5	1.401	800

Measurement Cases

Case 1	$\ddot{x}_1, \ddot{x}_2, \ddot{x}_3, \ddot{x}_4$ are measured
Case 2	$\ddot{x}_2$ and $\ddot{x}_4$ are measured

In summary, the proposed hybrid strategy consists of first identifying ground input from Section 2.3.1 using Equations (20) and (22), then applying Kalman filter to estimate state, $\hat{\mathbf{x}}_{[k|k]}$, and response at unmeasured location, $\hat{\mathbf{y}}_{[k|k]}$, using Equations (23)-(28). As a result, input, state, and response at unmeasured locations are obtained using a limited number of absolute floor acceleration measurements.

2.5. | Online joint state and input estimation

In this section, for comparison purpose, a state-of-the-art online method for unbiased minimum-variance input and state estimation that makes no assumption of the input, termed the Gillijns Algorithm,[25] is presented for systems without direct feedthrough. The algorithm is considered as an optimal filter. The proof of the optimality can be found in Ref. (25). The algorithm consists of three steps: time update, estimation of unknown input, and measurement update. The unknown ground input $\hat{\mathbf{u}}_{\mathbf{g}[\mathbf{k}]}$ is determined using the following equations:

$$\hat{\mathbf{x}}^*_{[k|k-1]} = \mathbf{A}_d\, \hat{\mathbf{x}}^*_{[k-1|k-1]}, \tag{29}$$

$$\hat{\mathbf{u}}_{g[k-1]} = \mathbf{M}_{[k]}(\mathbf{y}_{[k]} - \mathbf{C}_d\, \hat{\mathbf{x}}^*_{[k|k-1]}), \tag{30}$$

$$\hat{\mathbf{x}}^*_{[k|k]} = \hat{\mathbf{x}}^*_{[k|k-1]} + \mathbf{B}_d\hat{\mathbf{u}}_{g[k-1]} + \mathbf{K}^*_{[k]}(\mathbf{y}_{[k]} - \mathbf{C}_d\, \hat{\mathbf{x}}^*_{[k|k-1]} - \mathbf{C}_d\mathbf{B}_d\hat{\mathbf{u}}_{g[k-1]}), \tag{31}$$

where $\mathbf{M}_{[k]}$ and $\mathbf{K}^*_{[k]}$ are the input and state gain which are updated at each time k and $\hat{\mathbf{x}}^*_{[k|k]}$ is the state estimate vector.

From Equation (30), the unknown $\hat{\mathbf{u}}_{g[k-1]}$ is estimated with one time-step delay since measurement $\mathbf{y}_{[k]}$ at first step k doesn't have information about the input. The unbiasedness of $\hat{\mathbf{u}}_{g[k-1]}$ was obtained through the criterion $\mathbf{M}_{[k]}\mathbf{C}_d\mathbf{B}_d = \mathbf{I}$, and it is also assumed that $\mathbf{C}_d\mathbf{B}_d$ has full column. Further details of the algorithm are discussed in Ref. (25).

3. | NUMERICAL INVESTIGATION

3.1. | Numerical model

To investigate the accuracy and robustness of the proposed strategy, as shown in Figure 1, a numerical model of a four-story shear-type building structure is adopted. The floor mass and stiffness values are listed in the table shown in Figure 1. Four percent modal damping is assigned to all four modes of the structure. As shown in the figure, absolute accelerations are measured at each floor, which will be used to estimate the ground acceleration input as well as unmeasured floor responses. To assess the effect of incomplete measurements, two cases are considered including: Case 1—accelerations at all four floors are measured, and Case 2—accelerations are measured only at the 2nd and 4th floors.

Both modelling error and measurement noise are included when assessing the performance of the proposed method. For modeling error, considering the fact that the main source of error in analytical modeling is the deviation of structural parameters from their true values, modeling errors are introduced by increasing both the stiffness values and damping ratios by a certain percentage (up to 5%). Hence, modeling error is introduced as a deterministic bias from the true system,

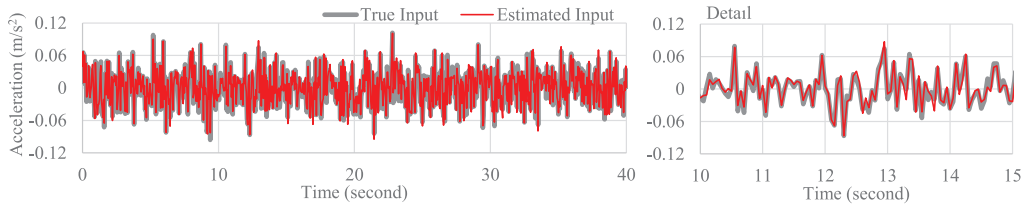

(a) Case 1: amplitude error = 6.5%, phase error = 3.2%, FDE = 9.7%

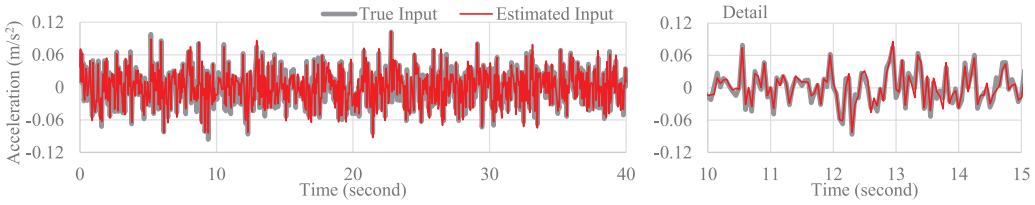

(b) Case 2: amplitude error =7.6%, phase error = 4%, FDE = 11.6%

FIGURE 2 Ground input estimation with 12% measurement noise and 5% modeling error

rather than a stochastic Gaussian process noise.[46] As a result, state estimation from Kalman filtering will no longer be optimal. The level of modeling error is limited to 5% since in practice model calibration/updating procedures are typically adopted to achieve such a level of accuracy. Moreover, various levels of measurement noise, up to 12%, in terms of root mean square (RMS) ratio are considered by adding zero-mean Gaussian white noise to the simulated absolute floor accelerations. Note that this study is not intended to investigate the upper bound of modeling error and measurement noise of the proposed method. The intention however is to demonstrate its robustness under substantial measurement noise and realistic modeling errors. To quantify the accuracy of the estimation results, both the amplitude error and phase error are calculated, the summation of which gives the frequency domain error (FDE).[47] Finally, to illustrate the robustness of the proposed method, the estimated ground input is compared with that of the online method presented in Section 2.5.

Two types of ground acceleration input, including stationary (band-limited white noise, or BLWN) and nonstationary (earthquake) ground inputs, are investigated. All ground inputs have a duration of 40 seconds and are sampled at 20 Hz. As described in Section 2.4, the proposed strategy first performs input estimation based on the measurement and model. The measurement vector $\mathbf{y}_{[k]}$ contains the absolute floor acceleration responses including measurement noise, for which two measurement cases are considered as shown in Figure 1. The model is described by matrices$\mathbf{A}_d$,$\mathbf{B}_d$, and $\mathbf{C}_d$, which are constructed from the structural parameters shown in Figure 1 after considering modeling errors. With the estimated input ground acceleration, Kalman filter is then applied to identify unmeasured floor responses such as accelerations, velocities, and displacements. Here, the initial state vector $\hat{\mathbf{x}}_{[0|-1]}$ for the Kalman filter is set to zero. $\mathbf{Q} = 10^{-1}\mathbf{I}$, $\mathbf{R} = 10^{-1}\mathbf{I}$, and $\mathbf{P}_{[0|-1]} = 10^{3}\mathbf{I}$, respectively.

3.2. | Stationary ground input: BLWN

In this section, the performance of the proposed strategy is assessed under a BLWN by considering different measurement noise, number of measurements and modelling error.

3.2.1. | Input estimation

The reconstructed input ground motions are shown in Figure 2 for both Case 1 (four-floor acceleration measurements) and Case 2 (two floor acceleration measurements). 12% measurement noise and 5% modeling error are considered in both cases. For Case 1 when all four-floor accelerations are measured, the estimated input has an FDE of 9.7%, which is comprised of 6.5% amplitude error and 3.2% phase error. In Case 2 when only two floor accelerations are measured, the FDE error increased slightly to 11.6%, including 7.6% amplitude error and 4% phase error. However, considering the 12% measurement noise and 5% percent modeling error, the estimated input still presents satisfactory accuracy, which can also be observed from the details presented in Figure 2.

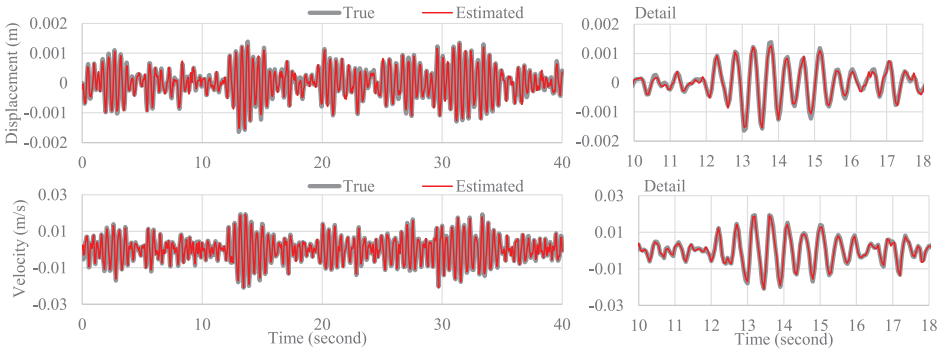

(a) Case 1: state estimations at the 4th floor
Amplitude error = 9.4%, phase error = 3.4%, FDE = 12.9%

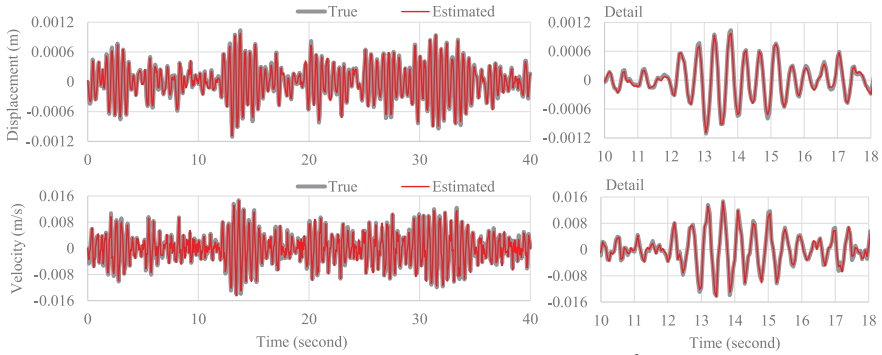

(b) Case 2: state estimations at the 3rd floor
Amplitude error = 4.3%, phase error = 2%, FDE = 6.3%

FIGURE 3 State (relative displacement and velocity) estimation with 12% measurement noise and 5% modeling error

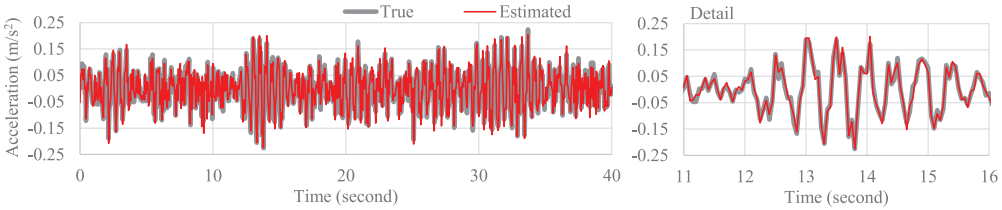

FIGURE 4 Estimated absolute acceleration at the unmeasured (3rd) floor in Case 2, with 12% measurement noise and 5% modeling error (amplitude error = 9%, phase error = 5.1%, FDE = 14.1%)

3.2.2. | State and unmeasured floor acceleration estimation

Figure 3 shows the state (velocity and displacement) estimation results using Kalman filter based on the input estimated from Section 3.2.1. Specifically, Figure 3A shows the estimated displacement and velocities at the 4th floor for Case 1, while Figure 3B illustrates the results for Case 2 at the 3rd floor, where no sensing information is used in state estimation. The associated FDEs are also shown in each figure. Overall, the estimated states agree very well with the true states, with 12.9% and 6.3% FDEs for Case 1 and Case 2, respectively. In addition, it is noted that incomplete floor acceleration measurements do not seem to have negative effect on state estimation, since the state estimation results for Case 2 have lower errors than Case 1. The results demonstrate the robustness of the proposed strategy in state estimation in the presence of limited measurements, measurement noise, and modelling error.

In addition to state estimation, for Case 2, absolute floor acceleration responses are estimated at unmeasured floors. Figure 4 shows the comparison between the true and the estimated absolute acceleration at the 3rd floor. The estimated response shows a good agreement with the true response with an FDE of 14.1% (9% amplitude error and 5.1% phase error). Overall, the proposed strategy achieved good performance in estimation of both states and responses at unmeasured locations.

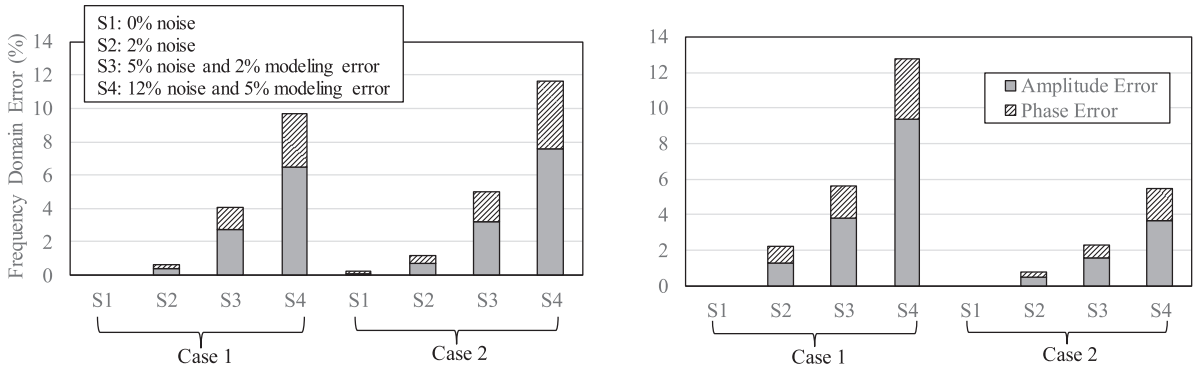

FIGURE 5 The frequency domain errors (FDE) under different scenarios of measurement noise and modeling error

3.2.3. | Impact of different levels of measurement noise and modeling error

The previous subsections showed the performance of the proposed strategy under a particular level of measurement noise (12%) and modeling error (5%). To investigate the impact of various levels of noise and error, in this section, the levels of measurement noise and modeling error for both Case 1 and Case 2 are varied, and the associated FDEs for input and state estimations are shown in Figure 5. First of all, when no measurement noise is present, full acceleration measurement (Case 1) achieved near perfect input and state estimations. However, when only partial floor acceleration measurements are available (Case 2), the estimated input shows a slightly higher error. On the other hand, the accuracies of state estimations are equally good between these two cases, indicating that incomplete measurement has higher impact on input estimation compared with state estimation. In fact, as shown in Figure 3B, the accuracy of state estimation is consistently higher in Case 2 when partial floor accelerations are used. This could be attributed to the fact that less noise is introduced by using a smaller number of noisy measurements.

3.3. | Nonstationary earthquake input: earthquake loading

In this section, the performance of the proposed input-state estimation strategy is investigated for nonstationary earthquake ground input. An earthquake ground motion measured during the 1994 Northridge earthquake from an instrumented building in Burbank, California is scaled and used in this investigation. Similar to the stationary input investigated in Section 3.2, the two measurement cases shown in Figure 1 are considered with 12% measurement noise and 5% modelling error.

3.3.1. | Input estimation

Figure 6 shows the estimated earthquake input for Case 1 and Case 2. The estimated nonstationary ground acceleration inputs show satisfactory agreements with the actual ground inputs for both cases. Similar to the case of stationary input, decreasing the number of measured floor accelerations (Case 2) leads to a slightly higher error in the input estimation result.

3.3.2. | State and unmeasured floor acceleration estimation

Using the estimated ground motion input from Section 3.3.1, the states of each floor and responses at unmeasured floors are estimated through Kalman filter. Figure 7A shows the estimated states (velocity and displacement) under 12% measurement noise and 5% modelling error at the 4th for Case 1, while Figure 7B shows the same information at the 3rd floor where no measurement was made for Case 2. Similar to the case of stationary ground input, the estimated states are very close to the true ones, yielding satisfactory FDEs. The error of state estimation for Case 2 is lower than Case 1.

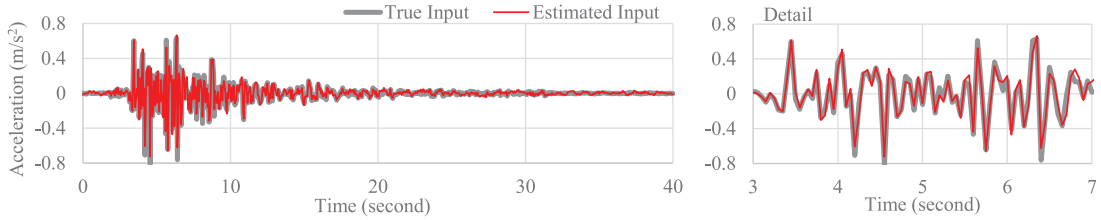

(a) Case 1: amplitude error = 7.3 %, phase error = 3.9%, FDE = 11.1%

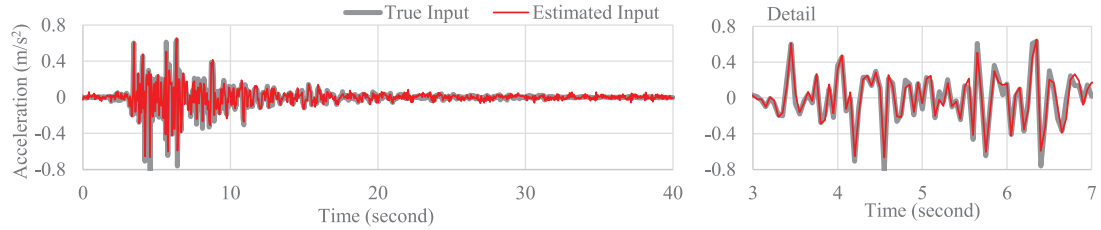

(b) Case 2: amplitude error = 9.5%, phase error = 5%, FDE = 14.5%

FIGURE 6 Nonstationary ground input estimation with 12% measurement noise and 5% modeling error

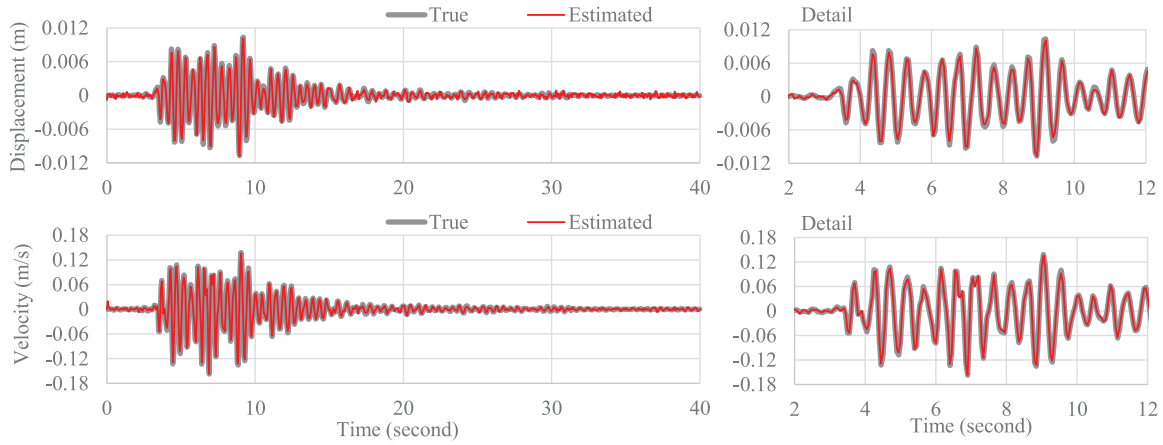

(a) Case 1: state estimation at the 4th floor (Amplitude error = 12%, phase error = 3.1%, FDE = 15.1%)

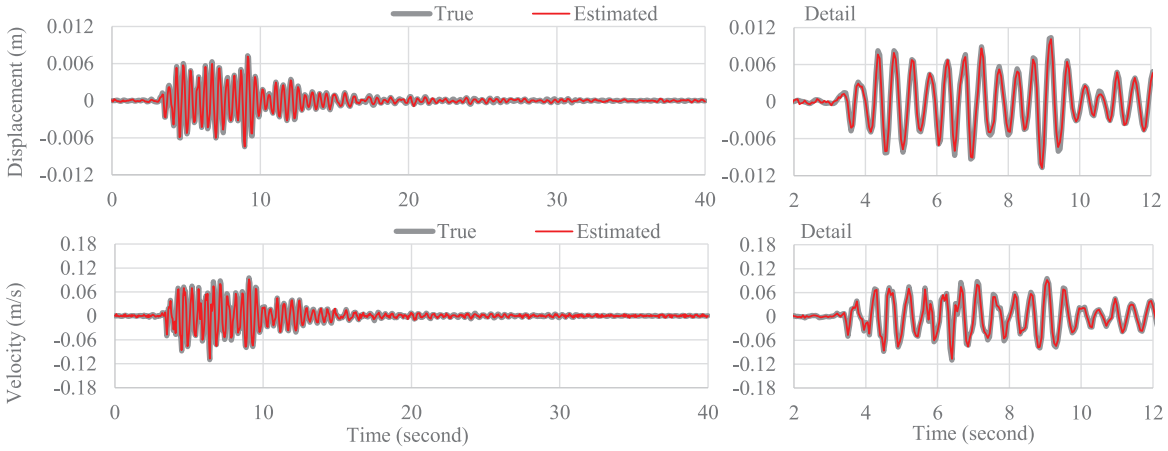

(b) Case 2: state estimation at the 3rd floor (Amplitude error = 5.4%, phase error = 2.2%, FDE = 7.6%)

FIGURE 7 State (relative displacement and velocity) estimation with 12% measurement noise and 5% modeling error

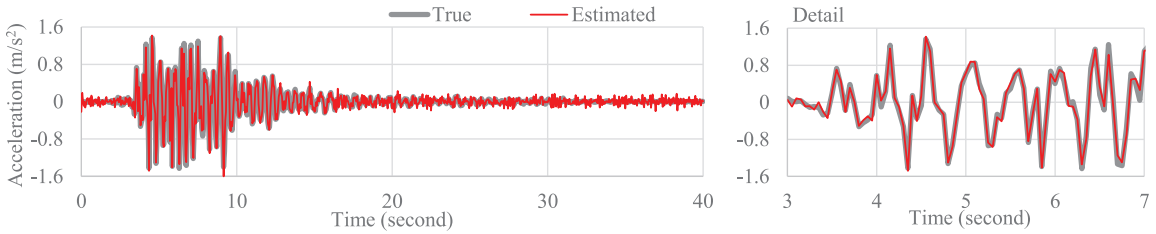

FIGURE 8 Estimated absolute acceleration at the unmeasured (3rd) floor in case 2, with 12% measurement noise and 5% modelling error (amplitude error = 11.2%, phase error = 6.1%. FDE = 17.3%)

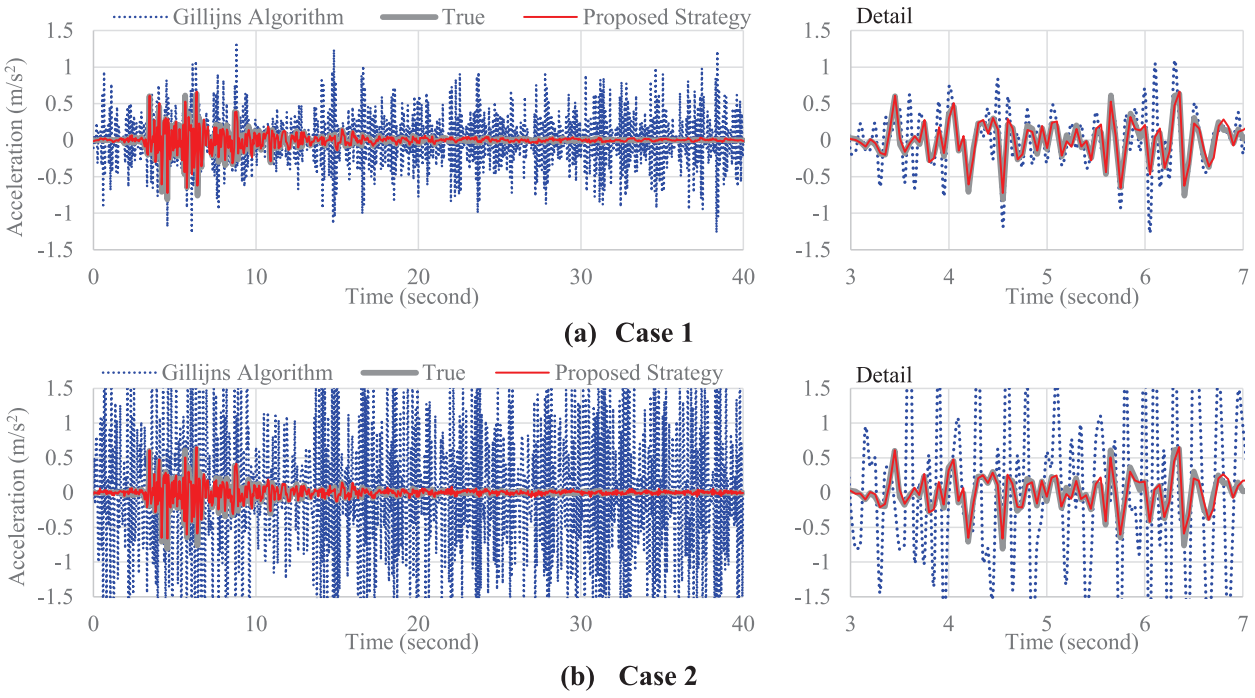

FIGURE 9 Nonstationary ground input estimations with 12% measurement noise and 5% modeling error

Once again, it shows that incomplete floor acceleration measurements do not seem to have negative effect on state estimation. Finally, the unmeasured acceleration at the 3rd floor is also estimated through Kalman filter. The result is shown in Figure 8. A good agreement is seen between the estimated and the true acceleration responses. Overall, the proposed strategy is shown effective for state and response estimation under nonstationary earthquake input, with similar level of FDEs observed from the stationary input case.

3.4. | Comparative study

In this section, the performance of the proposed strategy for input estimation is compared with the online method presented in Section 2.5, termed the Gillijns algorithm. In this comparison, both Case 1 and Case 2 are considered with 12% measurement noise and 5% modelling error. Figures 9A and 9B demonstrate the comparison of input estimation results between the Gillijns algorithm and the proposed strategy. Due to the weak observability of the ground input, unstable results are obtained using the online estimation method in the presence of given measurement noise and modeling error. On the other hand, the proposed hybrid strategy achieved stable input estimation even using incomplete floor acceleration measurements.

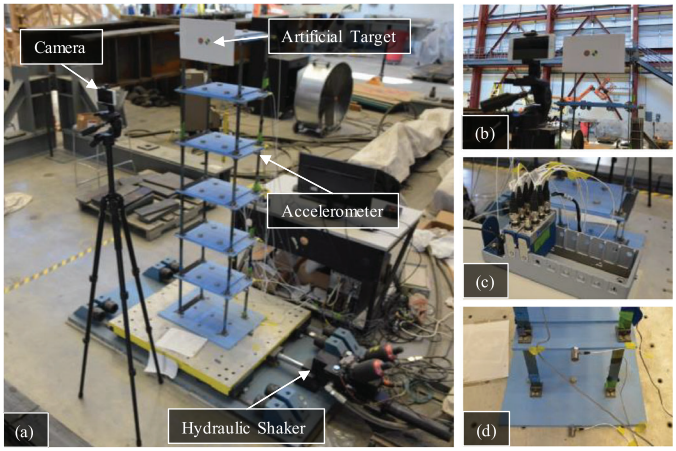

FIGURE 10 (A) The six-story laboratory building structure and measurement setup; (B) the smartphone camera and artificial target; (C) the DAQ system; and (D) the accelerometers installed on the shake table and the first floor

4. | EXPERIMENTAL INVESTIGATION

4.1. | Laboratory model and measurement setup

As shown in Figure 10, a six-story shear-type laboratory building structure was used to perform the experimental investigation. The structure was mounted on a hydraulic shake table at the University of Kansas for simulating earthquake excitation. Each floor of the building model consists of four steel columns ($12 \times 1.25 \times 0.125$ in, or $304.8 \times 31.75 \times 3.175$ mm) and one steel floor plates ($18 \times 12 \times 0.375$ in, or $457.2 \times 304.8 \times 9.525$ mm), which are connected together using bolts and angles. The mass of each of the first five floors is 20.3 kg, while is 19.3 kg for the sixth floor.

Figure 10 illustrates the measurement setup. Accelerations and displacements at the shake table and each floor were measured during the tests. Specifically, seven piezoelectric accelerometers with sensitivities around 100 mV/g were used to measure both the shake table and floor accelerations. Displacement of the shake table was measured by the LVDT (linear variable differential transformer) of the shake table actuator. To measure floor displacements for the later comparison of state estimation, a smartphone (iPhone 6) camera was used to measure the absolute displacement of the sixth floor through an iOS app, RINO (Real-time Image-processing for Noncontact mOnitoring) developed by Min et al.[48] An artificial target was installed at the sixth floor to enable real-time tracking of displacement with the smartphone.

During the tests, the acceleration data was sampled at 2048 Hz with a National Instruments (NI) CompactDAQ system, while the displacement data from the LVDT was sampled at 125 Hz. The absolute displacement of the sixth floor was measured at a frame rate of 120 fps and a resolution of 720 pixels with the smartphone. For the tests, the main earthquake excitation was followed by a sine wave, which served as the basis for synchronizing the various data collected with different methods. After data collection, all date sets were downsampled to 28 Hz, which is above twice the highest modal frequency of the structures. Finally, the relative displacement of the sixth floor is obtained by subtracting the ground displacement from the absolute floor displacement, which will serve as the reference for comparing the state estimation result.

4.2. | System identification and modeling using experimental data

As a model-based approach, the proposed strategy requires to establish the state space model, that is, the $\mathbf{A}_d$, $\mathbf{B}_d$, and $\mathbf{C}_d$ matrices for both input and state estimation. In this section, the state space model was estimated from the experimental data through system identification. Since this paper aims to estimate input, state, and responses at unmeasured locations in presence of modelling errors and incomplete measurements, the system model was identified using a direct approach based on only partial knowledge of experimental modal parameters. Here, only natural frequencies and damping ratios were utilized for the model calibration, which can be obtained through one of the cross power spectral density (CPSD) functions or the Frequency Response Functions (FRFs) of any floor. A BLWN ground excitation was applied to obtain the FRF of the third floor as shown in Figure 11, from which the experimental natural frequencies, f_{exp} and damping ratios, ζ_{exp}, based on the half-power method were identified. Table 1 summarizes the results of f_{exp} and ζ_{exp}. Note that other more advanced methods such as NExT-ERA,[49,50] N4SID/SSI[51] could also be applied to identify the modal parameters.

To construct the system model $[\mathbf{A}_d, \mathbf{B}_d, \mathbf{C}_d]$, the mass, $\mathbf{M}$, and stiffness, $\mathbf{K}$, matrices were first obtained from the physical parameters of the building including the geometry and the material properties of the structure, which can be obtained

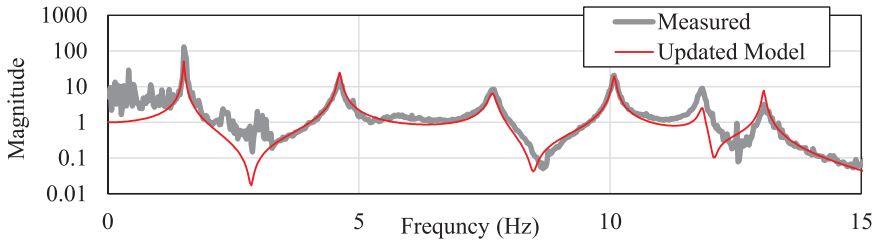

FIGURE 11 Comparison of the FRF magnitude between the measurement and the updated model for the lab structure

TABLE 1 Experimental natural frequencies, $\boldsymbol{f_{exp}}$, and damping ratios, $\boldsymbol{\zeta_{exp}}$

Mode no.	1	2	3	4	5	6
Natural frequency, $\boldsymbol{f_{exp}}$ (Hz)	1.5	4.6	7.7	10	11.8	13
Damping ratio, $\boldsymbol{\zeta_{exp}}$ (%)	0.8	0.6	0.8	0.3	0.4	0.21

from design or as-built drawings in practice. Next, the eigenvectors or model shapes, $\boldsymbol{\Phi}$, are determined from $\mathbf{M}$ and $\mathbf{K}$ matrices. Subsequently, the stiffness, $\mathbf{K}$, and damping, $\mathbf{C}$, matrices were updated through the direct approach based on the experimental modal frequencies and damping ratios as

$$\begin{aligned} \mathbf{K} = \boldsymbol{\Phi}^{-T}\mathbf{K}_r\boldsymbol{\Phi}^{-1} \quad \text{and} \quad \mathbf{C} = \boldsymbol{\Phi}^{-T}\mathbf{C}_r\boldsymbol{\Phi}^{-1}, \\ \mathbf{K}_r = \text{diag}\left(\omega_{exp,1}^2 M_1, \dots, \omega_{exp,6}^2 M_6\right), \\ \mathbf{C}_r = \text{diag}\left(2\zeta_{exp,1}\omega_{exp,1} M_1, \dots, 2\zeta_{exp,6}\omega_{exp,6} M_6\right), \end{aligned} \tag{32}$$

where $\mathbf{M}_r = \text{diag}(M_1, \dots, M_6) = \boldsymbol{\Phi}^T\mathbf{M}\boldsymbol{\Phi}$ is the modal mass matrix and $\omega_{exp,i} = 2\pi \boldsymbol{f_{exp,i}}$. As a result, $\mathbf{M}$, $\mathbf{C}$, and $\mathbf{K}$ matrices were identified for the building, followed by constructing the $\mathbf{A}_d$, $\mathbf{B}_d$, and $\mathbf{C}_d$ matrices. Figure 11 shows the comparison of the FRF magnitude of the third floor between the measurement and the updated system model. Note that the above procedure ensures close match of natural frequencies and damping ratios, but not mode shapes, as can be observed from the slight deviation in the FRF amplitudes at the peak locations. The discrepancy contributes to the modeling error which commonly exists in practical applications.

With the experimental system model $[\mathbf{A}_d, \mathbf{B}_d, \mathbf{C}_d]$, the proposed strategy described in Section 2.4 was applied to estimate the ground input, followed by estimation of floor states and unmeasured responses using Kalman filter with ground input estimated from the previous step. Here, the same values used in the numerical examples in Section 3 for the matrices $\mathbf{P}_{[0|-1]}$, $\mathbf{Q}$, and $\mathbf{R}$, were utilized, which are $10^3\mathbf{I}$, $10^{-1}\mathbf{I}$ and $10^{-1}\mathbf{I}$, respectively, and the initial state vector $\hat{\mathbf{x}}_{[0|-1]}$ was set to be zero.

4.3. | Joint input-state estimation based on earthquake input

One of the earthquake ground accelerations recorded during the Northridge earthquake of January, 1994 was used to run the test using the shake table. The nonstationary ground input was the recorded ground motion at the Burbank 6-story commercial building (CGS station 24370, Channel 9). The procedure defined in Section 4.1 was applied to collect data. To simulation partial instrumentation, only three absolute acceleration measurements at the 3rd, 5th, and 6th floors were applied in the input estimation. The remaining acceleration measurements at the 1st, 2nd, and 4th floors were used as references to compare with the corresponding response estimations. Similarly, the estimated ground input and floor displacements from the proposed strategy are compared with the measured ground input obtained from the accelerometer installed on the shake table and the reference relative displacement obtained from the smartphone and the LVDT, respectively.

4.3.1. | Ground input identification result

In this section, the experimental result for the estimated earthquake input using the proposed strategy is described. Figure 12 compares the estimated ground acceleration input with the measured one and shows the associated estimation

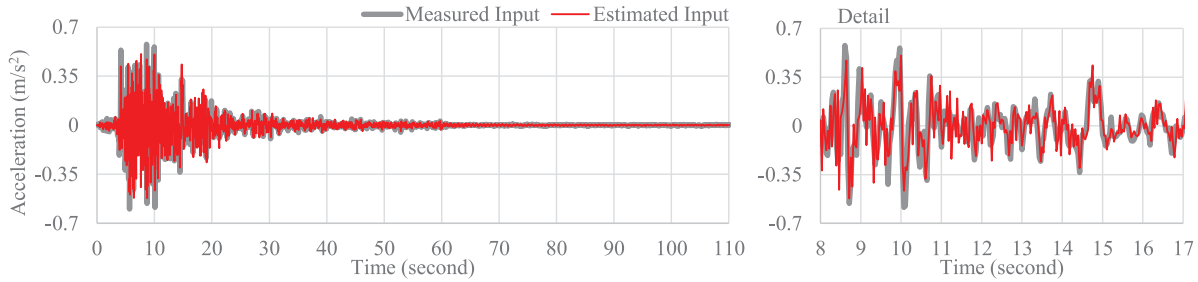

FIGURE 12 Earthquake input estimation result (amplitude error = 17.2%, phase error = 12.9%, FDE = 30.1%)

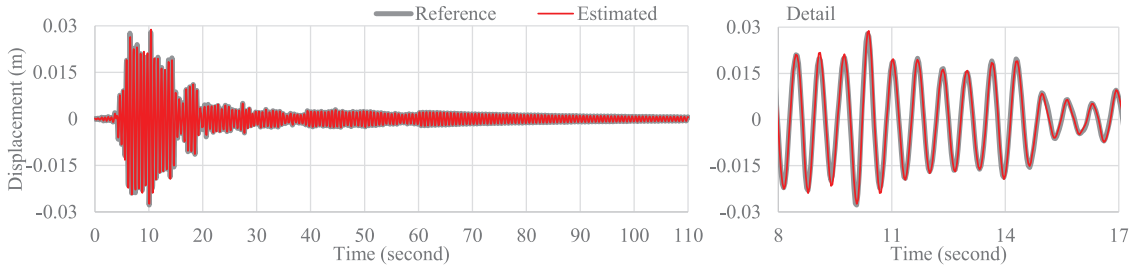

FIGURE 13 State (relative displacement) estimation at the 6th floor (amplitude error = 5.6 %, phase error = 7.5 %, FDE = 13.1%)

errors. Overall, the estimated input agrees well with the reference with an amplitude error of 17.2% and a phase error of 12.9%. Some amplitude and phase errors can be observed in the detailed picture especially at peaks, which could be attributed to modelling error since the numerical model was updated based on only experimental modal parameters obtained from the third floor, and lacks the knowledge of the experimental mode shapes. Considering the impact of modeling error, measurement noise, and partial floor measurements, a robust and satisfactory input estimation was achieved with the proposed strategy.

4.3.2. | State and unmeasured floor acceleration estimation

With the estimated input, the states and responses at unmeasured floors were further estimated using Kalman filter according to the proposed strategy. States including the relative floor displacements and velocities, and absolute acceleration responses at unmeasured floors were estimated using only three absolute acceleration measurements at the 3rd, 5th, and 6th floors. Figure 13 compares the estimated relative displacement at the 6th floor with the reference measured from the smartphone camera and the LVDT. Overall, the estimated relative floor displacement agrees well with the measured displacement, showing acceptable amplitude error (5.6 %) and phase error (7.5 %).

Similarly, the relative floor velocities were also estimated. Due to the lack of direct velocity measurements in the experimental program, the relative floor velocities estimated from Kalman filter with the measured ground acceleration input were used as reference for the comparison. As shown in Figure 14, the resulting amplitude and phase errors were 6.7%

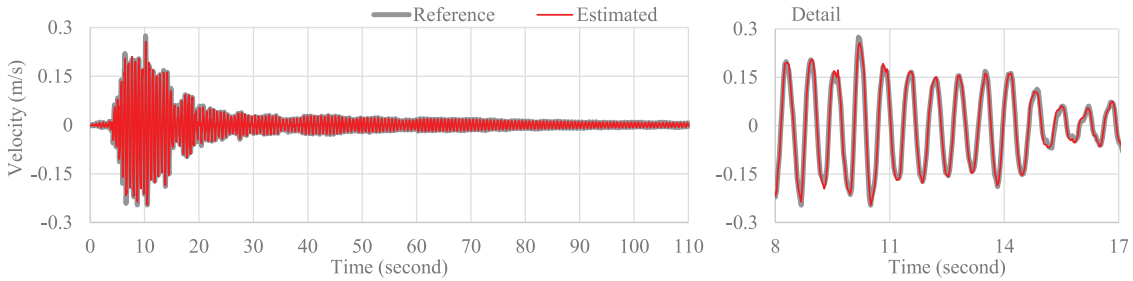

FIGURE 14 State (relative velocity) estimation at the 6th floor (amplitude error = 6.7%, phase error = 3.2%, FDE = 9.9%)

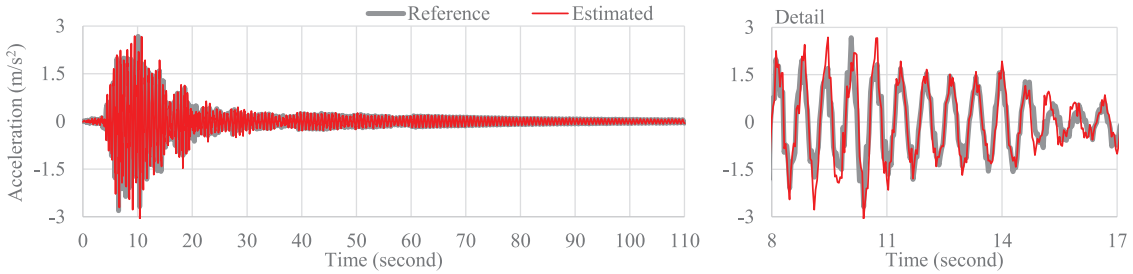

FIGURE 15 Unmeasured response estimation at the 4th floor (amplitude error = 24.6%, phase error = 16.4%, FDE = 41%)

FIGURE 16 A six-story building in Burbank, California, USA

and 3.2%, respectively, indicating very good agreement between the estimation and reference.

Finally, absolute acceleration responses at unmeasured floors were estimated. Figure 15 shows the estimated absolute acceleration response at the 4th floor using measurements at the 3rd, 5th, and 6th floors as well as the estimated input from the previous step. An acceptable result of the estimation is obtained, with 24.6% amplitude error and 16.4% phase error, though there is still discernable difference between the estimate and measured responses. Again, this difference could be attributed to the modelling error described in Section 4.2. Overall, satisfactory estimations for states and responses were obtained using experimental data, demonstrating the robustness of the proposed input-state strategy for earthquake-excited building structures in a practical setting.

5. | REAL-WORLD APPLICATION

5.1. | A Six-story buidling struture

This section presents the application of the proposed approach to an instrumented real-world building subject to earthquake loading. A six-story steel building located in Burbank, California, hereafter referred to as the Burbank building, was selected. As shown in Figure 16, the building was designed based on the 1973 Uniform Building Code (UBC) in 1976. The floors consist of 3-inch metal decking with a 3.25-inch lightweight concrete slab. W-sections were utilized for the columns and beams. The section dimensions for the columns and beams are shown in Figure 17. Further details of the building can be found in Ref. (52). Note that the internal columns only carry the vertical loads, whereas the perimeter frames are the primary lateral load resisting structures. Therefore, a 2D-model for one of the perimeter frames is built to represent the entire building structure under earthquakes.[53]

Thirteen acceleration channels were installed at the ground, 1st, 2nd, and 6th floors of the building by CSMIP in 1980. Several significant earthquakes were recorded. An overview of the sensor channel arrangements is shown in Figure 18. Two of the recoded earthquakes, the 1987 Whitter earthquake and the 1991 Sierra Madre earthquake, were selected for validating the proposed strategy. The data were downsampled from 50 Hz to 40 Hz for the subsequent analysis.

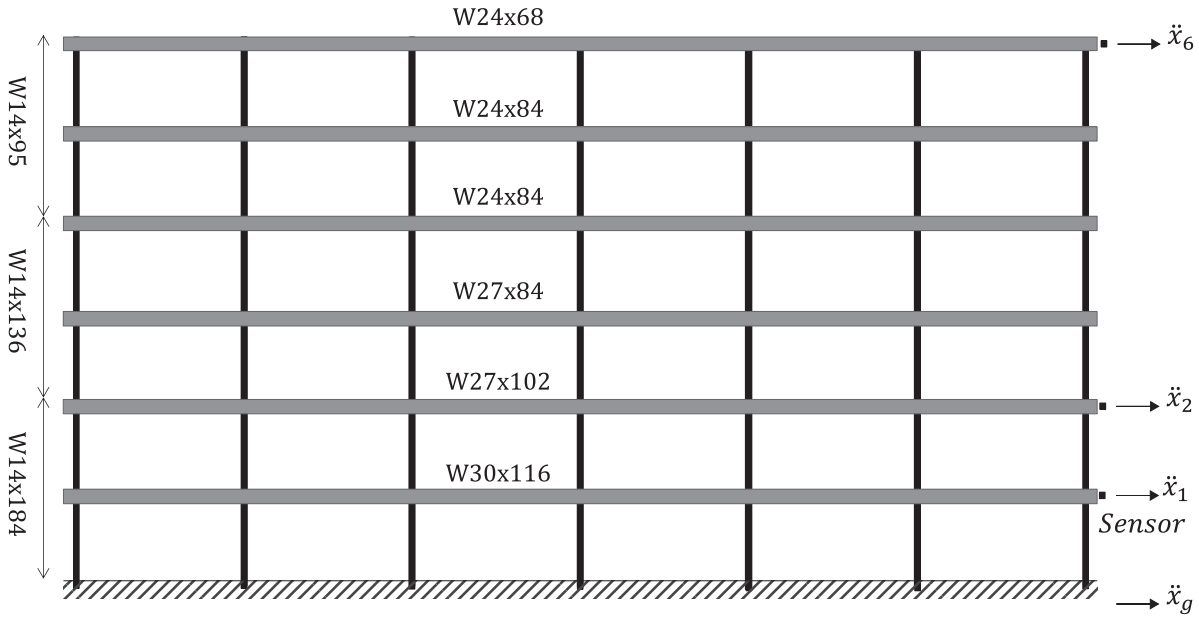

FIGURE 17 A lateral-load-resisting perimeter frame of the six-story building

FIGURE 18 Sensor arrangement and plan view of the perimeter frames of the building

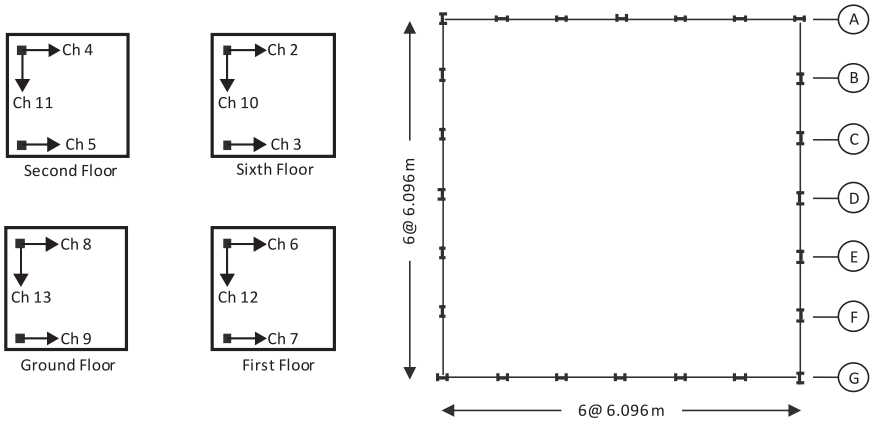

(a) Location of sensors (b) plan view of the building

5.2. | System identification

For the laboratory building structure presented in Section 4, modal information such as natural frequencies and damping ratios of all modes can be accurately identified using BLWN excitation, which can subsequently be used to calibrate the FE model. However, for the Burbank building, due to the transient nature of earthquake loading, system identification is intrinsically challenging and only two natural frequencies are identifiable,[53] as shown in Figure 19. As a result, modal calibration using the small number of identified modal properties does not yield adequate accuracy. Therefore, model calibration for the Burbank building was performed by directly using the time history data from the earthquake measurements. In particular, data measured during the 1991 Sierra Madre earthquake was used. An objective function formulated by the prediction error of floor acceleration responses was minimized through optimization by updating structural parameters that include stiffness, mass, and damping ratios. Subsequently, the updated state-space model is obtained from the structural parameters. Figure 19 compares the FRF magnitude of the sixth floor between the updated system model and measurements. The first two peaks of the FRF amplitudes match quite well. However, peaks corresponding to the remaining modes are not clear in the measurements. As a result, the accuracy of the updated model beyond the second mode cannot be verified, yielding uncertainties in the updated model.

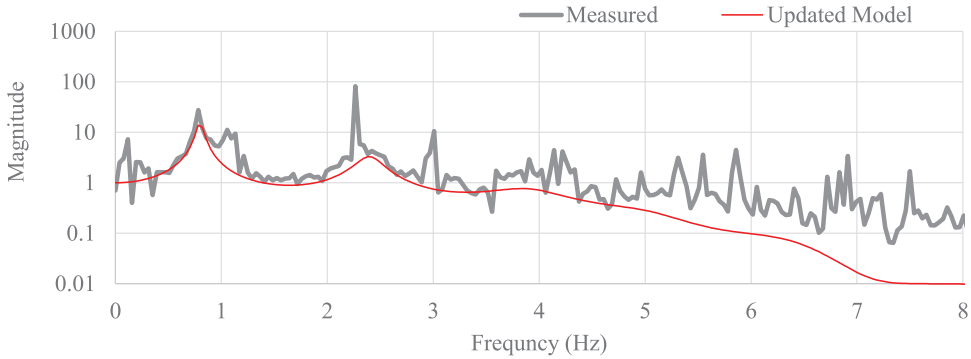

FIGURE 19 Comparison of the FRF magnitude between the updated model and the measurement for the Burbank Building (frequency up to 8 Hz is shown for clarity)

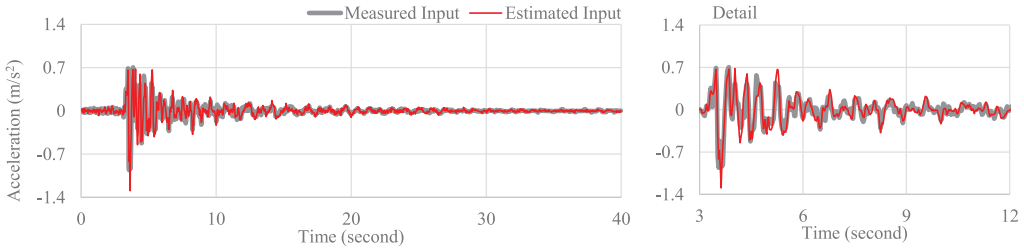

(a) The 1991 Sierra Madre earthquakes (Amplitude error = 15.7 %, phase error = 9.7 %, FDE = 25.4 %)

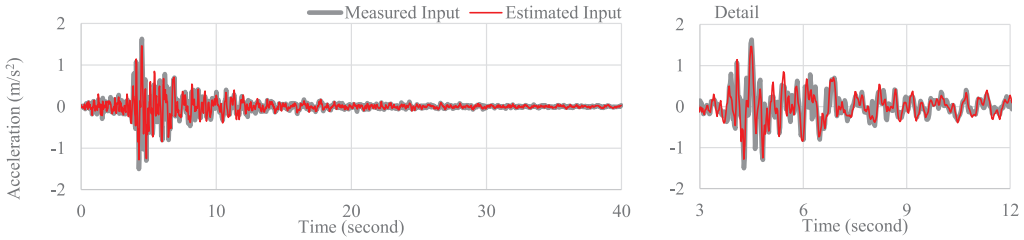

(b) The 1987 Whitter earthquakes (Amplitude error = 17.5 %, phase error = 8.7 %, FDE = 26.2 %)

FIGURE 20 Earthquake input estimation results for the Burbank building

5.3. | Joint input-state estimation for real earthquakes

The recoded data from both 1987 Whitter earthquake and 1991 Sierra Madre earthquake was used to validate the proposed method, with peak ground accelerations (PGA) equal to 0.22 g (2.16 m/s^2) and 0.11 g (1.08 m/s^2), respectively. In particular, measurements from Channels 8, 6, 4, and 2 that captured accelerations of the ground, 2nd, 3rd, and 6th floors were used for estimation and validation. Since incomplete floor accelerations are available for this particular building, only acceleration measurements at the 1st and 6th floors (Channels 6 and 2) were used to identify the ground input, followed by the estimation of displacement state and acceleration responses at all floors, including the unmeasured floors. To verify the results, the estimated ground input was compared with the measured one (Channel 8) and the estimated acceleration response at the 2nd floor was compared with the Channel 4 (see Figures 17 and 18A). The matrices $\mathbf{P}_{[0|-1]}$, $\mathbf{Q}$, and $\mathbf{R}$ of Kalman filter were selected as $10^3\mathbf{I}$, $10^{-1}\mathbf{I}$, and $10^{-1}\mathbf{I}$, respectively, the same as those used in the previous numerical and experimental examples.

5.3.1. | Ground input identification result for the Burbank building

In this section, the ground input was estimated using acceleration measurements at 1st and 6th floors. Figure 20 shows the estimation results for both earthquakes. For both cases, good accuracies were achieved in the estimated ground inputs, indicated by a 15.7% amplitude error and a 9.7% phase error for the 1991 Sierra Madre earthquake and a 17.5% amplitude

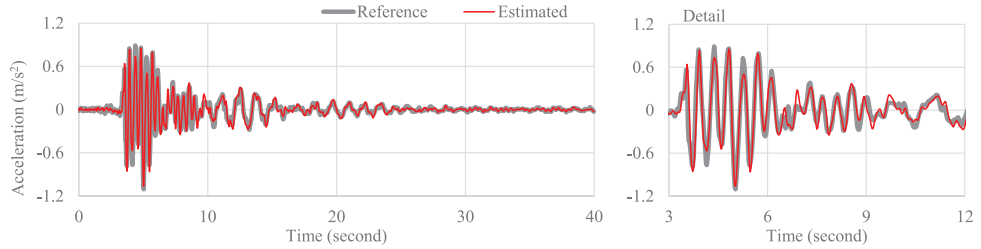

(a) The 1991 Sierra Madre earthquakes (Amplitude error = 14.5 %, phase error = 13.7 %, FDE = 28.2 %)

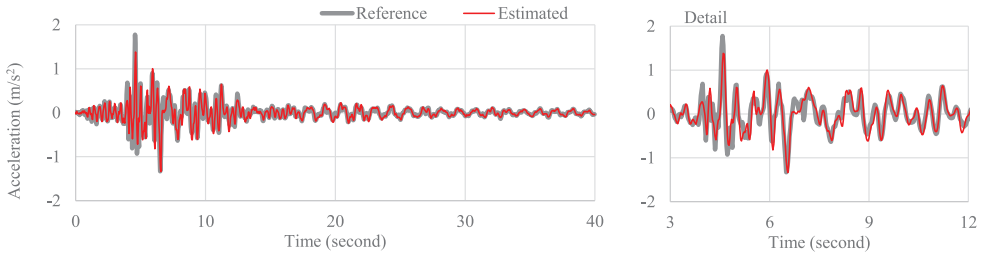

(b) The 1987 Whitter earthquakes (Amplitude error = 15.1 %, phase error = 16.9 %, FDE = 32 %)

FIGURE 21 Acceleration response estimation at the 2nd floor

error and an 8.7% phase error for the 1987 Whitter earthquakes. The discrepancies as shown in the details can be partially attributed to the modeling error because the updated model was based on the short period vibration data recorded during the earthquakes, which lacks enough knowledge about modal parameters of the building. Overall, the ground acceleration inputs for both earthquakes were successfully reconstructed in presence of uncertainties including modelling error, measurement noise, and incomplete response measurements, indicating the effectiveness and robustness of the proposed strategy for input estimation of real building structures.

5.3.2. | Floor acceleration response identification result for the Burbank building

As mentioned previously, measured acceleration responses were available at 1st, 2nd, and 6th floors, but only those at 1st and 6th floors were used for the input estimation. This was done on purpose such that the remaining measurement at 2nd floor (Channel 4) could be utilized to testify the proposed strategy in terms of estimating responses at unmeasured locations. To this end, the Kalman filter described in Section 2, specifically Equation (26), was applied to identify the acceleration responses at all floors. Figure 21A compares the estimated acceleration responses at 2nd floor with the corresponding measured accelerations (Channel 4) for 1991 Sierra Madre earthquakes. The estimated acceleration matches well with the reference with an amplitude error of 14.5% and a phase error of 13.7%. Similar performance for the 1987 Whitter earthquake is also shown in Figure 21B. Again, the errors observed in the figure could be partially attributed to the modelling errors caused by the lack of enough knowledge about higher modes using the short period vibration data. Better result can potentially be achieved by improving the model updating process, which leads to a more accurate model. The ability to estimate acceleration responses at unmeasured floors brings significant benefit to current strong motion database such as CSMIP, in which most instrumented buildings had sensors at limited number of floors.

5.3.3. | State (displacement) identification result for the Burbank building

In addition to the ground input and floor acceleration response estimation, the result of the state (displacement) estimation using only two floor acceleration measurements at 1st and 6th floor is demonstrated here. Figures 22 and 23 illustrate the estimated displacement for both earthquakes at 2nd and 6th floors. Note that acceleration measurement at 2nd floor was not used in the estimation. Due to the lack of real displacement measurements in real earthquake events, only the estimated displacements are shown here. Since the performance of the proposed strategy for statement estimation was validated in the experimental investigation in Section 4.3.2 where reference displacements were available, the estimated

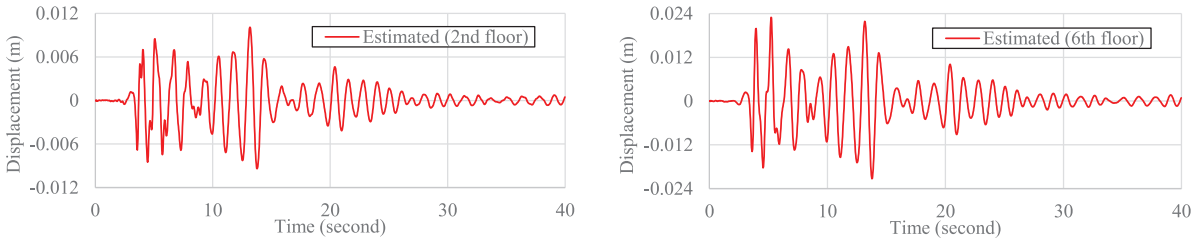

FIGURE 22 Floor state (relative displacement) estimation for the 1991 Sierra Madre Earthquake

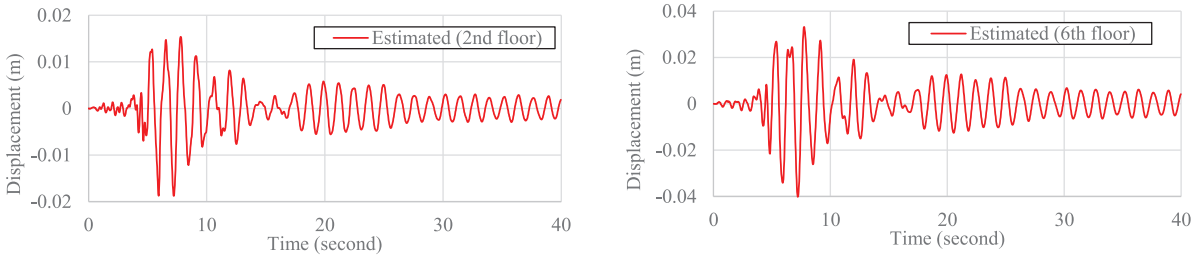

FIGURE 23 Floor state (relative displacement) estimation for the 1987 Whitter Earthquake

displacements for the Burbank building shown in Figures 22 and 23 can be utilized for many engineering purposes such as postearthquake structural assessment.

6. | CONCLUSIONS

This paper investigated input and state estimation for earthquake-excited building structures using incomplete absolute floor acceleration response measurements. The major challenge of input-state estimation, in this case, stems from the lack of direct feedthrough in the system due to the utilization of responses in terms of absolute floor accelerations. As a result, the system is weakly observable for its input. The contribution of this paper is the proposed strategy to estimate input and state for systems without direct feedthrough despite the issue of input observability. The main contributions and conclusions are summarized as follows.

In the context of estimating input, state, and responses at unmeasured locations, the mathematical formulation of the proposed two-step strategy was presented for systems without direct feedthrough, with particular attention placed on earthquake-excited building structures and absolute floor acceleration measurements. In the first step, input is estimated using the maximum *a posteriori* (MAP) approach. In the second step, the Kalman filter in conjunction with the identified input from the first step is employed to estimate states and responses at unmeasured locations. In order to compare the proposed strategy with existing online model-based methods, the online method for systems without direct feedthrough, the Gillijns Algorithm, was introduced. Moreover, the formulation of observability of system input was introduced to further illustrate and highlight the challenge.

The performance of the proposed strategy was first demonstrated through a numerical example with a four-story shear-type building structure, with consideration of both stationary (BLWN) and nonstationary (earthquake) ground inputs, different levels of measurement noise and modelling error, and number of measured floors. The results indicate the proposed strategy achieved robust and satisfactory accuracy in the estimations under realistic levels of modeling error and measurement noise, as well as partial measurements. It was also found that incomplete measurement has higher impact on input estimation compared with state estimation.

In addition, the proposed strategy was compared with the Gillijns Algorithm under both full and partial measurements. While the online method suffered from large error and unstable estimation results under modeling error and measurement noise due to weak observability, the proposed strategy was shown able to overcome the challenge and achieve robust and satisfactory accuracy.

Subsequently, an experimental program was carried out with a scaled six-story laboratory structure for further assessment. The numerical model was obtained through experimental data with a direct updating strategy using modal

frequencies and damping, but not mode shape information, leaving noticeable modeling error. A smartphone camera was utilized along with an artificial mark to collect displacement measurements at the top floor for reference purpose. The proposed strategy achieved robust and satisfactory accuracy in the estimation of input, states, and unmeasured floor responses using experimentally obtained partial floor acceleration measurements.

Finally, one of the instrumented buildings by CSMIP was selected for real-world assessment of the proposed strategy using two recorded earthquake events, including the 1987 Whitter earthquake and the 1991 Sierra Madre earthquake. Only a limited number of floors were instrumented for absolute acceleration measurement. Using accelerations only measured at the 1st and 6th floors, the ground acceleration input and responses at unmeasured floors were successfully reconstructed with satisfactory accuracy, demonstrating the applicability and performance of the proposed strategy under real-world settings. Future work will investigate optimal sensor placement strategies for the proposed method.

ORCID

Jian Li https://orcid.org/0000-0003-3439-7539

REFERENCES

1. Housner GW. Historical view of earthquake engineering. *Proceedings of the Eighth World Conference on Earthquake Engineering*. Englewood Cliffs, NJ: Prentice-Hall 1986.
2. Lin S, Li J, Elnashai AS, Spencer Jr. BF. NEES integrated seismic risk assessment framework (NISRAF). *Soil Dyn Earthquake Eng*. 2012;42:219–228.
3. Goltz JD, ed. The Northridge, California earthquake of January 17, 1994: general reconnaissance report. Rep. No. NCEER-94-0005. *National Center for Earthquake Engineering Research*. Buffalo, NY: University at Buffalo–State Univ. of New York; 1994.
4. FEMA-356. Prestandard and Commentary for the Seismic Rehabilitation of Building. Washington, DC: Federal Emergency Management Agency; 2000.
5. Xiang P, Nishitani A, Marutani S, et al. Identification of yield drift deformations and evaluation of the degree of damage through the direct sensing of drift displacements. *Earthquake Eng Struct Dynam*. 2016;45(13):2085–2102.
6. Skolnik DA, Wallace JW. Critical assessment of interstory drift measurements. *J Struct Eng*. 2010;136(12):1574–1584.
7. McCallen D, Petrone F, Coates J, Repanich N. A laser-based optical sensor for broad-band measurements of building earthquake drift. *Earthquake Spectr*. 2017;33(4):1573–1598.
8. Islam MN, Zareie S, Alam MS, Seethaler RJ. Novel method for interstory drift measurement of building frames using laser-displacement sensors. *J Struct Eng*. 2016;142(6):06016001.
9. Kalman RE. A new approach to linear filtering and prediction problems. *J Basic Eng*. 1960;82(1):35–45.
10. Zonta D, Wu H, Pozzi M, et al. Wireless sensor networks for permanent health monitoring of historic buildings. *Int J Smart Struct Syst*. 2010;6(5-6):595–618.
11. Bard P-Y, Riepl-Thomas J. Wave propagation in complex geological structures and their eects on strong ground motion. In: Kausel E, Manolis GD (eds.). *Wave Motion in Earthquake Engineering*. Boston: International Series Advances in Earthquake Engineering, WIT; 1999: 37–95.
12. Ghahari SF, Abazarsa F, Taciroglu E. Identification of soil-structure systems. In: Limongelli M, Çelebi M (eds.). *Seismic Structural Health Monitoring*. Springer Tracts in Civil Engineering. Cham: Springer; 2019. https://doi.org/10.1007/978-3-030-13976-6_6.
13. Jie L, Jun C. A statistical average algorithm for the dynamic compound inverse problem. *Comput Mech*. 2003;30(2):88–95.
14. Zhao X, Xu YL, Li J, Chen J. Hybrid identification method for multi-story buildings with unknown ground motion: theory. *J Sound Vib*. 2006;291(1):215–239.
15. Zhao X, Xu YL, Chen J, Li J. Hybrid identification method for multi-story buildings with unknown ground motion: experimental investigation. *Eng Struct*. 2005;27(8):1234–1247.
16. Lourens E, Reynders E, De Roeck G, Degrande G, Lombaert G. An augmented Kalman filter for force identification in structural dynamics. *Mech Syst Sig Process*. 2012;27:446–460.
17. Naets F, Cuadrado J, Desmet W. Stable force identification in structural dynamics using Kalman filtering and dummy-measurements. *Mech Syst Sig Process*. 2015;50-51:235–248.
18. Khodabandeloo B, Melvin D, Jo H. Model-based heterogeneous data fusion for reliable force estimation in dynamic structures under uncertainties. *Sensors*. 2017;17(11):2656.
19. Gillijns S, De Moor B. Unbiased minimum-variance input and state estimation for linear discrete-time systems with direct feedthrough. *Automatica*. 2007;43(5):934–937.
20. Lourens E, Papadimitriou C, Gillijns S, Reynders E, De Roeck G, Lombaert G. Joint input-response estimation for structural systems based on reduced-order models and vibration data from a limited number of sensors. *Mech Syst Sig Process*. 2012;29:310–327.
21. Fang H, Shi Y, Yi J. On stable simultaneous input and state estimation for discrete-time linear systems. *Int J Adapt Control Signal Process*. 2011;25(8):671–686.
22. Maes K, Smyth AW, De Roeck G, Lombaert G. Joint input-state estimation in structural dynamics. *Mech Syst Sig Process*. 2016;70-71:445–466.

23. Maes K, Van Nimmen K, Lourens E, Rezayat A, Guillaume P, De Roeck G, Lombaert G. Verification of joint input-state estimation for force identification by means of in situ measurements on a footbridge. *Mech Syst Sig Process*. 2016;75:245–260.
24. Azam SE, Chatzi E, Papadimitriou C. A dual Kalman filter approach for state estimation via output-only acceleration measurements. *Mech Syst Sig Process*. 2015;60-61:866–886.
25. Gillijns S, De Moor B. Unbiased minimum-variance input and state estimation for linear discrete-time systems. *Automatica*. 2007;43(1):111–116.
26. Tuan PC, Ji CC, Fong LW, Huang WT. An input estimation approach to on-line two-dimensional inverse heat conduction problems. *Numer Heat Transfer*. 1996;29(3):345–363.
27. Liu JJ, Ma CK, Kung IC, Lin DC. Input force estimation of a cantilever plate by using a system identification technique. *Comput Meth Appl Mech Eng*. 2000;190(11):1309–1322.
28. Ma CK, Chang JM, Lin DC. Input forces estimation of beam structures by an inverse method. *J Sound Vib*. 2003;259(2):387–407.
29. Wu AL, Loh CH, Yang JN, Weng JH, Chen CH, Ueng TS. Input force identification: application to soil–pile interaction. *Struct Control Health Monitor*. 2009;16(2):223–240.
30. Nayek R, Chakraborty S, Narasimhan S. A Gaussian process latent force model for joint input-state estimation in linear structural systems. *Mech Syst Sig Process*. 2019;128:497–530.
31. Ding Y, Law SS, Wu B, Xu GS, Lin Q, Jiang HB, Miao QS. Average acceleration discrete algorithm for force identification in state space. *Eng Struct*. 2013;56:1880–1892.
32. Liu K, Law SS, Zhu XQ, Xia Y. Explicit form of an implicit method for inverse force identification. *J Sound Vib*. 2014;333(3):730–744.
33. Zhu XQ, Law SS, Bu JQ. A state space formulation for moving loads identification. *J Vib Acoust*. 2006;128(4):509–520.
34. Feng D, Sun H, Feng MQ. Simultaneous identification of bridge structural parameters and vehicle loads. *Comput Struct*. 2015;157:76–88.
35. Sun H, Büyüköztürk O. Identification of traffic-induced nodal excitations of truss bridges through heterogeneous data fusion. *Smart Mater Struct*. 2015;24(7):075032.
36. Wang J, Zabaras N. Hierarchical Bayesian models for inverse problems in heat conduction. *Inverse Problems*. 2005;21(1):183–206.
37. Jin B, Zou J. A Bayesian inference approach to the ill-posed Cauchy problem of steady-state heat conduction. *Int J Numer Methods Eng*. 2008;76(4):521–544.
38. Jin B, Zou J. Augmented Tikhonov regularization. *Inverse Problems*. 2008;25(2):025001.
39. Hansen PC. Analysis of discrete ill-posed problems by means of the L-curve. *SIAM Rev*. 1992;34(4):561–580.
40. Krener AJ, Ide K. Measures of unobservability. *IEEE Conference on Decision and Control*. Shanghai, China; 2009: 6401–6406.
41. Taher S, Li J, Fang H. Input and state estimation for earthquake-excited building structures using acceleration measurements. In *Sensors and Smart Structures Technologies for Civil, Mechanical, and Aerospace Systems 2018* (Vol. 10598, p. 1059827). Denver, CO: International Society for Optics and Photonics; March, 2018.
42. Juang JN. Applied system identification. *Englewood Cliffs*. NJ, USA: Prentice Hall; 1994.
43. MATLAB. Version 9.5.0.944444 (R2018b). Natick, Massachusetts: The MathWorks Inc.; 2018.
44. Simon D. *Optimal State Estimation: Kalman, H∞, and Nonlinear Approaches*. Hoboken, New Jersey: John Wiley & Sons; 2006.
45. Welch G, Bishop G. An introduction to the Kalman filter. Chapel Hill, NC: UNC-Chapel Hill, TR 95-041; July 26, 2006.
46. Carrassi A, Vannitsem S, Nicolis C. Model error and sequential data assimilation: a deterministic formulation. *Q J R Meteorolog Soc*. 2008;134(634):1297–1313.
47. Dragovich JJ, Lepage A. FDE index for goodness-of-fit between measured and calculated response signals. *Earthquake Eng Struct Dynam*. 2009;38(15):1751–1758.
48. Min JH, Gelo NJ, Jo H. Non-contact and real-time dynamic displacement monitoring using smartphone technologies. *J Life Cycle Reliab Saf Eng*. 2015;4(2):40–51.
49. James GH, Carne TG, Lauffer JP. The natural excitation technique (NExT) for modal parameter extraction from operating structures. *Modal Anal: Int J Anal Exp Modal Anal*. 1995;10:260–277.
50. Juang J-N, Pappa RS. An eigensystem realization algorithm for modal parameter identification and model reduction. *J Guid, Contr, Dynam*. 1985;8(5):620–627.
51. Van Overschee P, De Moor B. N4SID: subspace algorithms for the identification of combined deterministic-stochastic systems. *Automatica*. 1994;30(1):75–93.
52. Anderson JC, Bertero VV. Seismic performance of an instrumented six-story steel building (Vol. 91, No. 11). *Berkeley, California: Earthquake Engineering Research Center*. University of California at Berkeley; 1991.
53. Lin SL, Li J, Elnashai AS, Spencer Jr. BF. NEES integrated seismic risk assessment framework (NISRAF). *Soil Dyn Earthquake Eng*. 2012;42:219–228.

How to cite this article: Taher SA, Li J, Fang H. Earthquake input and state estimation for buildings using absolute Floor accelerations. *Earthquake Engng Struct Dyn*. 2020;1–23. https://doi.org/10.1002/eqe.3382